

Comprehensive Summaries of Uppsala Dissertations  
from the Faculty of Science and Technology 1035



# Atomic Layer Deposition of Copper, Copper(I) Oxide and Copper(I) Nitride on Oxide Substrates

BY

TOBIAS TÖRNDAHL



ACTA UNIVERSITATIS UPSALIENSIS  
UPPSALA 2004

Dissertation presented at Uppsala University to be publicly examined in Högssalen, The Ångström Laboratory, Uppsala, Friday, November 26, 2004 at 10:15 for the degree of Doctor of Philosophy. The examination will be conducted in English.

**Abstract**

Törndahl, T. 2004. Atomic Layer Deposition of Copper, Copper(I) Oxide and Copper(I) Nitride on Oxide Substrates. Acta Universitatis Upsaliensis. *Comprehensive Summaries of Uppsala Dissertations from the Faculty of Science and Technology* 1035. 57 pp. Uppsala. ISBN 91-554-6081-X

Thin films play an important role in science and technology today. By combining different materials, properties for specific applications can be optimised. In this thesis growth of copper, copper(I) oxide and copper(I) nitride on two different substrates, amorphous SiO<sub>2</sub> and single crystalline  $\alpha$ -Al<sub>2</sub>O<sub>3</sub> by the so called Atomic Layer Deposition (ALD) techniques has been studied. This technique allows precise control of the growth process at monolayer level on solid substrates. Other characteristic features of ALD are that it produces films with excellent step coverage and good uniformity even as extremely thin films on complicated shaped substrates.

Alternative deposition schemes were developed for the materials of interest. It was demonstrated that use of intermediate water pulses affected the deposition pathways considerably. By adding water, the films are thought to grow via formation of an oxide over-layer instead of through a direct reaction between the precursors as in the case without water.

For growth of copper(I) nitride from Cu(hfac)<sub>2</sub> and ammonia no film growth occurred without adding water to the growth process. The Cu<sub>3</sub>N films could be transformed into conducting copper films by post annealing. In copper growth from CuCl and H<sub>2</sub> the water affected film growth on the alumina substrates considerably more than on the fused silica substrates. The existence of surface -OH and/or -NH<sub>x</sub> groups was often found to play an important role, according to both theoretical calculations and experimental results.

*Keywords:* Atomic Layer Deposition, ALD, copper, copper(I) oxide, copper(I) nitride, deposition pathway, CuCl, Cu(hfac)<sub>2</sub>, oxide substrates, epitaxy, DFT, ab-initio

*Tobias Törndahl, Department of Materials Chemistry, Box 538, Uppsala University, SE-75121 Uppsala, Sweden*

© Tobias Törndahl 2004

ISSN 1104-232X

ISBN 91-554-6081-X

urn:nbn:se:uu:diva-4651 (<http://urn.kb.se/resolve?urn=urn:nbn:se:uu:diva-4651>)

# List of publications

This thesis is based on the following publications, which will be referred to in the text by their roman numerals.

- I. Atomic layer deposition of copper(I) oxide from copper(I) chloride and water**  
T. Törndahl, M. Ottosson, K. Larsson and J.-O. Carlsson  
In manuscript
- II. Growth of copper metall by atomic layer deposition using copper(I) chloride, water and hydrogen as precursors**  
T. Törndahl, M. Ottosson and J.-O. Carlsson  
Thin Solid Films, 458 (2004) 129.
- III. Epitaxy of copper on  $\alpha$ -Al<sub>2</sub>O<sub>3</sub>(001) by atomic layer deposition**  
T. Törndahl, J. Lu, M. Ottosson and J.-O. Carlsson  
In manuscript
- IV. Growth of copper(I) nitride by atomic layer deposition using copper(II) hexafluoroacetylacetonate, water and ammonia as precursors**  
T. Törndahl, M. Ottosson and J.-O. Carlsson  
In manuscript
- V. Formation of metallic copper by annealing of atomic layer deposition grown copper(I) nitride thin films**  
T. Törndahl, M. Ottosson and J.-O. Carlsson  
In manuscript
- VI. A theoretical study of copper(I) chloride adsorption on the (111) and (110) surfaces of copper(I) oxide**  
T. Törndahl, J.-O. Carlsson and K. Larsson  
In manuscript

## Comments on my contributions

Outlining and performing film depositions [I-V] and calculations [VI]. Film characterisation and evaluation of acquired data, except the TEM analysis in [III], SEM analysis in [IV] and operating the XPS in [I-II, IV]. Main author of the papers.

## Abbreviations and acronyms

ALCVD	Atomic Layer Chemical Vapour Deposition
ALD	Atomic Layer Deposition
ALE	Atomic Layer Epitaxy
CASTEP	CAMbridge Sequential Total Energy Package
CBED	Convergent Beam Electron Diffraction
CVD	Chemical Vapour Deposition
DFT	Density Functional Theory
EDS	Energy Dispersive Spectroscopy
FWHM	Full Width at Half Maximum
GI-XRD	Grazing Incidence X-Ray Diffraction
MBE	Molecular Beam Epitaxy
NC	Normally Closed
NO	Normally Open
PVD	Physical Vapour Deposition
QCM	Quartz Crystal Microbalance
RSM	Reciprocal Space Mapping
SAED	Selective Area Electron Diffraction
SEM	Scanning Electron Microscopy
TEM	Transmission Electron Microscopy
XPS	X-ray Photoelectron Spectroscopy
XRD	X-Ray Diffraction
XRFS	X-Ray Fluorescence Spectroscopy
XRR	X-Ray Reflectivity

# Contents

<b>1 Introduction</b> .....	<b>1</b>
<b>2 Methodology</b> .....	<b>3</b>
2.1 Experimental .....	3
2.1.1 Precursor selection .....	4
2.1.2 ALD reactors.....	5
2.1.3 Film characterisation methods .....	8
2.2 Computational methods .....	9
<b>3 Film growth and characterisation</b> .....	<b>11</b>
3.1 Copper(I) oxide .....	12
3.1.1 Film growth and characterisation.....	13
3.2 Copper metal.....	16
3.2.1 Film growth.....	17
3.2.2 Aspects of epitaxy .....	19
3.3 Copper(I) nitride.....	24
3.3.1 Film characterisation .....	25
3.3.2 Annealing of grown Cu <sub>3</sub> N films.....	28
<b>4 Growth mechanisms</b> .....	<b>31</b>
4.1 Copper(I) oxide .....	31
4.1.1 Experimental.....	31
4.1.2 DFT calculations .....	33
4.2 The effect and use of intermediate water pulses .....	38
4.2.1 The CuCl/H <sub>2</sub> O/H <sub>2</sub> process .....	38

4.2.2 The Cu(hfac) <sub>2</sub> /H <sub>2</sub> O/NH <sub>3</sub> process .....	40
<b>5 Summary and concluding remarks .....</b>	<b>46</b>
<b>6 Acknowledgements .....</b>	<b>49</b>
<b>7 Svensk sammanfattning .....</b>	<b>50</b>
<b>8 References .....</b>	<b>53</b>

# 1 Introduction

Thin films are used in a variety of applications, such as catalysis for increasing reaction rates of chemical processes, films for gas sensing properties, dielectric materials in the semi-conductor industry, conducting layers for metallisation applications, wear resistant films for cutting tools, solar cell applications, magnetic layers for data storage and so on. To be able to produce thin films with desired properties, good knowledge of the film growth processes is needed. There exist a large number of different deposition techniques to produce the thin layers. The applied methods spans from PVD methods, where the reactants are usually supplied to the surface that is to be coated as elements in atomic or ionic form to films deposited from the liquid by electrochemical methods. Furthermore, chemical methods such as CVD and ALD exist and are readily used. In CVD and ALD film growth is controlled by chemical reactions on or in the vicinity of the substrates surfaces.

The films in this work were deposited by the ALD technique, also known as ALE or ALCVD. ALD is a chemical deposition method like the more well-known related method, CVD [1, 2]. In both methods film deposition takes place from reactants in the vapour that have been transported into the film deposition zone. The difference between the two methods can be traced to how the precursors are supplied to the deposition zone. ALD is a pulsed process where the reactants are fed into the reactor separately and sequentially, whereas the reactants in CVD are transported into the deposition zone simultaneously and continuously. An inherent advantage of the precursor pulsing in ALD is that homogeneous reactions in the gas phase can be avoided. The ALD method was invented in the 1970s by Suntola [3]. Today the method is a well-known deposition technique, described in thin film synthesis text books [4, 5]. The considerable interest in the ALD method for modern day applications is high due to the fact that the method is known to produce films with excellent step coverage and good uniformity even at extremely thin films on complicated shaped substrates. One drawback with the ALD method is that the film growth rate is low as compared to other deposition methods such as CVD.

In this thesis, growth kinetics for ALD of copper and copper containing compounds, like  $\text{Cu}_2\text{O}$  and  $\text{Cu}_3\text{N}$  have been studied. The deposition processes have been performed on two different oxide substrates by using two different copper containing precursors. It is known that deposition of

non-oxide films can be problematic in ALD processes on oxide surfaces, for example, due to poor nucleation and/or adhesion. The aim of this work is to study such processes and investigate different deposition pathways for film growth of metallic copper and copper(I) nitride. In the following chapters, the deposition processes are described in detail.

## 2 Methodology

This chapter describes the film deposition and characterisation methods used in this thesis. Details regarding deposition system as well as the theoretical framework behind the ab-initio calculations are also given.

### 2.1 Experimental

A general overview of the ALD concept is given in Figure 2.1 for an ALD cycle describing film growth of a binary compound. It can be seen that the process is divided into four steps. Firstly, a precursor is supplied into the deposition zone from the vapour through transport in an inert carrier gas flow. The precursor then adsorbs on the surface by forming more or less strong chemical bonds with the surface atoms present.

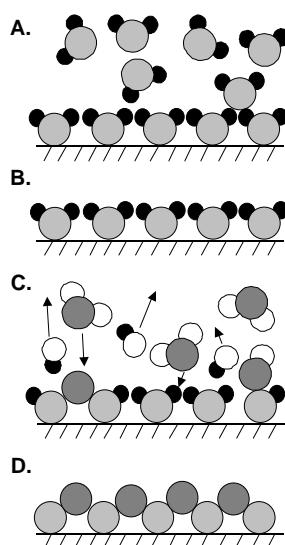


**Figure 2.1.** Typical ALD pulse sequence for deposition of a binary compound.

After the precursor pulse, the surface is covered by chemisorbed adsorbates (Figure 2.1a). (If the deposition temperature is low enough, physisorbed species may also exist on the surface.) Secondly, the reactor is flushed with inert carrier gas, typically argon or nitrogen gas, to remove excess precursor

from the surface (Figure 2.1b). In a third step, the second precursor is admitted into the reactor, and film growth takes place by a reaction between the two precursors, either on or in the vicinity of the surface (Figure 2.1c). Finally, the reactor is purged with inert gas to remove the reaction products formed during the previous step and excess precursor (Figure 2.1d). Thus, after the four steps an amount of film has been deposited on the surface. Ideally, one ALD cycle should generate one monolayer of film. However, this is seldom the case due to for example precursor repulsion leading to a smaller amount of precursor on the substrate surface or by precursor desorption. The ALD cycle is then repeated a given number of times to generate a film with desired thickness.

### 2.1.1 Precursor selection

Chemical film deposition processes are controlled by the choice of source materials. The chosen precursors can exist in the solid state, as liquids or in the vapour state. All precursors used in ALD need to be transported into the reactor in the vapour. This means that liquids must be vapourised, whereas solid state precursors need to be sublimated. The precursor flux is controlled by heating or cooling the precursor to achieve a suitable vapour pressure. Generally, solid state precursors have the lowest vapour pressures at lower temperatures. In ALD, two major precursor groups are the metal-organic (MO) and the halide precursors (for the metal source). The MO-precursors are usually more volatile than the halides, which lead to the fact that lower deposition temperatures can be employed. One problem that is frequently encountered when using the MO-precursor is higher film contamination due to cracking of the precursor ligands. On the other hand, employing halides generally leads to lower film contamination at the cost of using a higher deposition temperature. Furthermore, etch effects can be a problem in halide processes, where the produced reaction product reacts with the previously grown film.

In this work, two copper containing precursors have been used to grow copper(I) oxide, copper metal and copper(I) nitride films. The first copper precursor was copper(I) chloride, a copper halide. CuCl was chosen because it has the highest vapour pressure of the copper halides at the lowest possible temperature. CuCl may exist as monomers up to tetramers in the vapour depending on the reactor temperature. Film deposition by using the CuCl precursor can be viewed as a high temperature process. (The melting point of CuCl is 430 °C [6] and the precursor was sublimated at a temperature of 340 °C.) Cu<sub>2</sub>O and Cu were deposited with the CuCl precursor together with water and hydrogen gas at deposition temperatures ranging from 350 °C and upwards.

The second copper containing precursor was copper(II) hexafluoroacetylacetonate-hydrate [Cu(1,1,1,5,5,5-hexafluoro-2,4-pentanedionate)<sub>2</sub>], a

MO-precursor of copper(II)  $\beta$ -diketonate type. A sketch of  $\text{Cu}(\text{hfac})_2$  is shown in Figure 2.2.

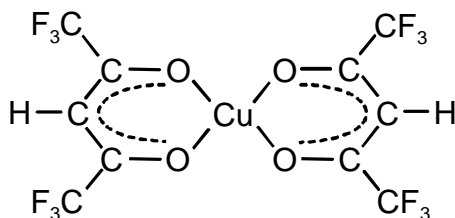


**Figure 2.2.** The  $\text{Cu}(\text{hfac})_2$  precursor.

The  $\text{Cu}(\text{hfac})_2$  precursor was chosen due to its low sublimation temperature ( $60\text{ }^\circ\text{C}$ ) and high reactivity. However, the precursor contains a small amount of water as crystal water. Therefore, it is imperative to investigate the effect of the crystal water because otherwise, the process may be influenced by a CVD contribution if the precursors are mixed during the  $\text{Cu}(\text{hfac})_2$  pulse. However, the outcome is not entirely clear when the effect of the crystal water was studied in the literature by mass spectroscopy [7, 8]. Moreover, it has been reported that  $\text{Cu}(\text{hfac})_2$  undergoes thermal decomposition under adsorption on surfaces at temperatures above  $300\text{ }^\circ\text{C}$  [9, 10]. A thorough investigation of the effects of the presence of the crystal water on the deposition process was carried out in [IV]. From XRFS, it was found that the rate of the possible film growth by mixing of the precursors or by thermal decomposition was less than  $0.005\text{ \AA/s}$  at  $247\text{ }^\circ\text{C}$ . At  $302\text{ }^\circ\text{C}$  signs of thermal decomposition of the precursor was observed. Films of  $\text{Cu}_2\text{O}$ ,  $\text{Cu}_3\text{N}$  and  $\text{Cu}$  were deposited with the  $\text{Cu}(\text{hfac})_2$  precursor together with water and ammonia. The lowest deposition temperature was  $210\text{ }^\circ\text{C}$ . Finally, a description of precursor choices in previous works, reported in the literature is given chapter 3.

### 2.1.2 ALD reactors

Film growth studies have been carried out in two different ALD reactors. The first ALD reactor is a smaller three-zone hot wall system, based on three silica tubes. Reactor one was used for all film depositions where the  $\text{CuCl}$  precursor was employed as copper source. The films were grown in the last reactor zone downstream and the  $\text{CuCl}$  precursor was sublimated into the first zone at a temperature of  $340\text{ }^\circ\text{C}$ . Together with  $\text{CuCl}$ , water and hydrogen were also available as precursors in the system. In all processes, water was evaporated from a glass vessel and the evaporation rate was controlled by a thermo-bath. Furthermore, argon was used as carrier gas. The Ar flow was distributed between three silica tubes to obtain the characteristic gas pulsing for the ALD process. A schematic picture of ALD-reactor one

and the general layout of the gas mixing can be seen in Figure 2.3. A total of two different substrate holders were used in the system, one titanium substrate holder that had been annealed in nitrogen gas to create an inert TiN surface and one  $\alpha$ -Al<sub>2</sub>O<sub>3</sub> crucible.

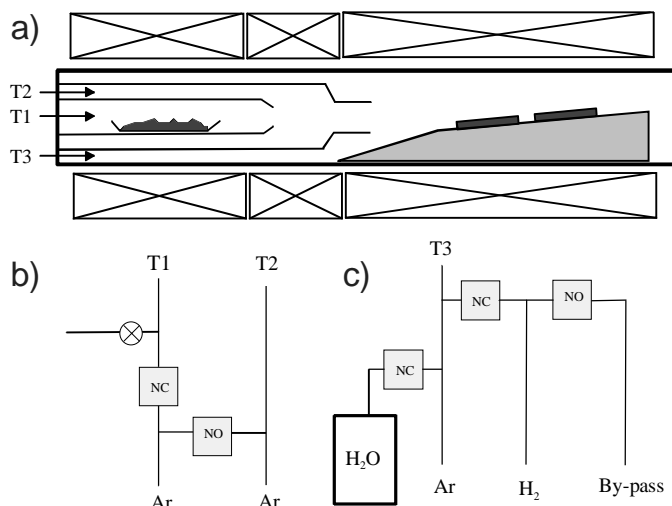


**Figure 2.3.** a) Schematic picture of ALD reactor one, b) pulse line controlling the CuCl flux and c) valve positions for controlling the H<sub>2</sub>O and H<sub>2</sub> doses.

The gas mixing in the system was governed by five pneumatic valves. Two valves controlled the CuCl pulsing, one valve the H<sub>2</sub>O pulsing and two valves controlled the H<sub>2</sub> pulsing. CuCl was transported to the deposition zone when an argon carrier flow passed through the innermost silica tube (T1 in Figure 2.3a). Accordingly, to hinder the CuCl supply, the Ar flow in T1 was switched to the central silica tube (T2 in Figure 2.3a). Furthermore, the gas flows were arranged in such a way that a small back flow over the precursor boat was utilised to abruptly abort the CuCl admission during the ALD process (Figure 2.3b). The water and hydrogen precursors were carried into the system through the outermost tube (T3 in Figure 2.3a). The water was supplied by effusion and governed by a pneumatic valve that opened and closed an evaporator (see Figure 2.3c). Finally, the hydrogen pulsing was arranged in such a way that the gas was either admitted into the system or via a main bypass line to the system pump side (Figure 2.3c).

Two deposition schemes were carried out in ALD reactor one. Firstly, film growth of Cu<sub>2</sub>O on amorphous SiO<sub>2</sub> and single crystalline  $\alpha$ -Al<sub>2</sub>O<sub>3</sub>(102) substrates by using a CuCl:Ar:H<sub>2</sub>O:Ar pulse sequence [I]. Secondly, growth of Cu metal on SiO<sub>2</sub> and  $\alpha$ -Al<sub>2</sub>O<sub>3</sub>(001) by applying CuCl:Ar:H<sub>2</sub>O:Ar:H<sub>2</sub>:Ar and CuCl/Ar/H<sub>2</sub>/Ar pulse sequences [II]. Some general process data are

given in Table 2.1. For a more thorough description of the processes, the reader is guided to the corresponding papers.

**Table 2.1.** Deposition parameters for the ALD processes.

Reactor	Phase	Precursors	P <sub>tot</sub> (Torr)	T <sub>dep</sub> (°C)	Pulse sequence (s)	Paper
1	Cu <sub>2</sub> O	CuCl/H <sub>2</sub> O	8	350-700	4:2:2:2	[I]
1	Cu	CuCl/H <sub>2</sub> O/H <sub>2</sub>	8	375-475	4:4:4:4:8:4	[II]
1	Cu	CuCl/H <sub>2</sub>	8	375-475	4:4:-:-:8:12	[III]
2	Cu <sub>3</sub> N, Cu	Cu(hfac) <sub>2</sub> /H <sub>2</sub> O/NH <sub>3</sub>	5	210-302	4:8:4:8:4:8	[IV]
2	Cu <sub>3</sub> N	Cu(hfac) <sub>2</sub> /NH <sub>3</sub>	5	247	4:8:-:-:4:8	[IV]

The second ALD reactor is basically an up-scaled version of the smaller reactor (see Figure 2.4). All film deposition where the Cu(hfac)<sub>2</sub> precursor was used as copper source was carried out in reactor two, which is a five-zone hot wall ALD-reactor with a 60 mm silica reactor tube. Cu(hfac)<sub>2</sub> was sublimated in the first two zones, while gas mixing and film growth occurred in the last zone. The reactants were transported into the deposition zone in five separate silica tubes in order to avoid gas mixing before the deposition zone. Instead, gas mixing occurred in a substrate block, placed in the deposition zone. The substrate block was made of nitrided titanium (TiN surface layer) in order to obtain a non-reactive surface. The metal block also gave a uniform temperature profile in the deposition zone. Of the five lines, three were designed for sublimation of solid precursors and two lines with a constant carrier gas flow for supply of other gaseous precursors such as water (admitted via G2 in Figure 2.4) and ammonia (admitted via G1 in Figure 2.4). Five pneumatic valves, two for Cu(hfac)<sub>2</sub>, one for water and two for ammonia controlled pulsing of reactants into the growth region in a similar fashion as described for the precursor pulsing in reactor one. The Cu(hfac)<sub>2</sub> precursor was sublimated at a temperature of 60 °C and supplied into the system by S1 (Figure 2.4). Prior to film deposition the Cu(hfac)<sub>2</sub> precursor was heat-treated for 30 min at the sublimation temperature in order to remove the hydrate water. Argon was used as carrier gas in the five silica tubes leading into the substrate block. Also, a bulk flow of argon was used outside the substrate block to obtain a flow in the main reactor tube. Both Cu<sub>3</sub>N and Cu were grown in reactor two by using Cu(hfac)<sub>2</sub>:Ar:H<sub>2</sub>O:Ar: NH<sub>3</sub>:Ar and Cu(hfac)<sub>2</sub>:Ar:NH<sub>3</sub>:Ar pulse sequences [IV]. Some general deposition parameters for the Cu(hfac)<sub>2</sub> processes are displayed in Table 2.1. More information about the experimental parameters is provided in [IV].

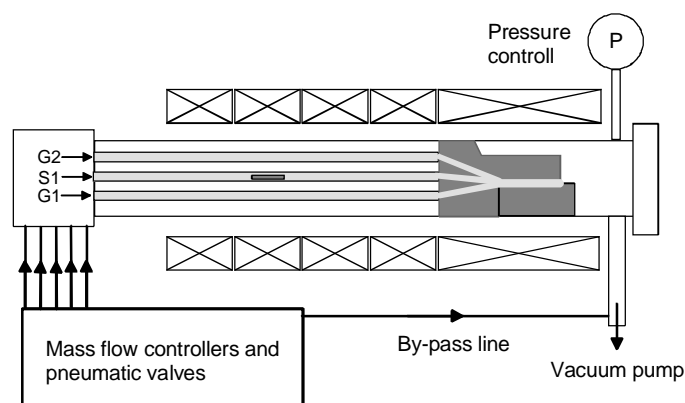


**Figure 2.4.** Schematic picture of the second ALD reactor.

### 2.1.3 Film characterisation methods

The deposited films have been characterised by numerous film analysis techniques (see Table 2.2). Some methods, where calibration with standards has been performed are discussed briefly below.

**Table 2.2** Applied film analysis methods.

Information	Analysis method	Paper
Phase	XRD, $\theta$ -2 $\theta$ and GI	[I-V]
Film thickness	XRFS	[I-V]
Film impurities	XPS	[I-II, IV]
Morphology	SEM	[I-II, IV]
Microstructure	TEM	[III]
Film orientation	XRD, pole figures	[III, V]
Cell parameters, strain, stress	XRD, RSM	[III]
Density, roughness, thickness	XRR	[IV]
Resistivity	Four-point probe	[V]
Growth rate, in-situ studies	QCM	-

One of the most commonly used techniques was energy dispersive XRFS for film thickness measurements. In these measurements, different targets were used to scatter X-ray radiation from a rhodium tube onto the sample. Depending on the choice of target, different excitation profiles are readily obtained. From XRFS the relative amount of deposited material can be obtained by integrating the intensities of characteristic peaks from the included elements. However, if an absolute thickness value is desired from XRFS, standards of known thicknesses have to be used. In all papers film thickness values are calculated from the integrated area of the Cu  $K_{\alpha}$  peak. The measured intensities were then compared to intensities from copper standards prepared by evaporation of copper on soda lime glass. Depending

on which phase that was deposited, the obtained film thickness values obtained by using the standards were multiplied by the density quotient between copper and the density of the deposited films. In the case of  $\text{Cu}_2\text{O}$ ,  $\rho(\text{Cu})/\rho(\text{Cu}_2\text{O})$  was used to obtain the corresponding  $\text{Cu}_2\text{O}$  thickness, whereas  $\rho(\text{Cu})/\rho(\text{Cu}_3\text{N})$  was used for the  $\text{Cu}_3\text{N}$  films. The density of the deposited films was assumed to be that of the bulk material. Finally, no absorption corrections were needed due to the fact that the films were thin.

The growth rates and possible deposition pathways have also been examined in-situ by QCM for the  $\text{Cu}(\text{hfac})_2/\text{H}_2\text{O}/\text{NH}_3$  and  $\text{Cu}(\text{hfac})_2/\text{NH}_3$  processes. In QCM, mass change on a crystal surface can be measured as a function of resonant frequency [11]. To be able to obtain absolute mass values, a calibration using the well-known  $\text{Al}(\text{CH}_3)_3/\text{H}_2\text{O}$  process [12] was performed. It was found that 1Hz corresponded  $7.7 \text{ ng/cm}^2$ . Prior to the QCM measurements a layer of  $\text{Al}_2\text{O}_3$  was grown on the crystal gold surface to stop reactions between  $\text{Cu}(\text{hfac})_2$  and the crystal surface. After the  $\text{Al}_2\text{O}_3$  layer had been applied, a 150 nm thick layer of  $\text{Cu}_3\text{N}$  was deposited by running the system in CVD mode. All mass values were calculated from the average of nine consecutive ALD cycles.

For quantitative determination of the chemical composition of the film impurities by XPS, new sensitivity factors have to be calculated from a compound of known composition. To calculate the level of oxygen impurities in  $\text{Cu}_3\text{N}$  films, a CVD grown  $\text{Cu}_2\text{O}$  standard with a non-detectable level of impurities was used [IV].

## 2.2 Computational methods

Ab-initio modelling can be used to give additional information about experimental processes. The scope of the calculations in this thesis is to give an understanding of the ALD growth process from  $\text{CuCl}$  and  $\text{H}_2\text{O}$ . All calculations were based on DFT, which is a well-known theory and has been described in many textbooks and papers [13, 14]. The calculations were performed within the CASTEP package [15], with the Perdew and Wang PW91 functional [16]. Ultra-soft pseudopotentials were used as representation of the atoms. Furthermore, the calculations were based on a super-cell approach by using plane wave basis sets, where the k-point sampling in the Brillouin zone was generated by a Monkhorst-Pack scheme [17].

In a first step, two  $\text{Cu}_2\text{O}$  surfaces, (111) and (110), were prepared by geometry optimisations. Thereafter, model and basis set size, together with other parameters such as k-point sampling was optimised to give a good accuracy for a  $\text{CuCl}$  adsorption process on the two surfaces. A more thorough description of the test calculations can be found in [VI]. To model different possible ALD film growth pathways, total energies for different

surface reactions and adsorption processes were calculated on the previously optimised Cu<sub>2</sub>O surfaces according to:

$$\Delta E_{react} = E_{slab} + E_{ads} - E_{slab+ads} - E_{prod} \quad (2.1)$$

where  $\Delta E_{slab}$  is defined as the total energy of the surface and possible adsorbates prior to reaction.  $E_{ads}$  is the total energy of the incoming reactant that may interact with surfaces or with the surface adsorbed species.  $E_{slab+ads}$  is the total energy for the surface with possible attached reaction products, whereas  $E_{prod}$  is the total energy for desorbed reaction products. Furthermore, by the definition in eq. 2.1 the total reaction energy  $\Delta E_{react}$  is more exothermic the higher the total energy for the overall reaction is.

### 3 Film growth and characterisation

Films of copper(I) oxide, copper(I) nitride and copper metal have been deposited by ALD on two oxide substrates, amorphous  $\text{SiO}_2$  and single crystalline  $\alpha\text{-Al}_2\text{O}_3$ . Growth of non-oxide films on oxide substrates has been found to be difficult by ALD. One problem can be attributed to the initial nucleation process. It is known from the literature that addition of water to an ALD/CVD process can be used to increase film growth rate, which has been demonstrated for CVD growth of metallic copper [18-20]. To find an alternative ALD process for growth of non-oxide films on oxide substrates, the concept of adding an intermediate water pulse is evaluated for growth of  $\text{Cu}_3\text{N}$  and Cu. The effect of adding water in the process sequence is compared to film deposition where the water was excluded from the ALD scheme. Hence, an ALD pulse sequence with water included, consisted of six steps as compared to four steps in a water free process. In the water-based processes, two major steps are thought to be included during the growth reaction. Firstly, a reaction between the copper precursor and water to form an oxide layer on the substrate/film surface occurs. Secondly, a step where the newly formed oxide layer is consumed in a surface reaction with a third precursor (ammonia or hydrogen gas), and the  $\text{Cu}_3\text{N}$  or Cu phase is obtained. Hence, in theory, a new oxide layer will be formed during each subsequent ALD cycle. One important criterion for the intermediate reaction gas (water in this case) is that it does not react with the previously formed nitride/metal. In the water free process,  $\text{H}_2/\text{NH}_3$  reacted directly with the copper precursors.

Two copper sources were used, copper(I) chloride and copper(II) hexafluoroacetylacetonate [ $\text{Cu}(\text{hfac})_2$ ]. The deposition schemes including CuCl as copper source can be regarded as a high temperature process as compared to film deposition where  $\text{Cu}(\text{hfac})_2$  was used as copper precursor. In a first reaction step, common for the two precursors, copper(I) oxide could be grown by adding water to the ALD pulse sequence. The growth of  $\text{Cu}_2\text{O}$  has also been studied [I, IV] since it can give valuable information of the first reaction between the copper-containing precursor and water in the multistep growth processes of both copper metal and copper(I) nitride. To produce  $\text{Cu}_3\text{N}$  films, ammonia was added as a third precursor [IV], whereas hydrogen gas [III] or ammonia [IV, V] could be used to grow films of copper metal. A schematic overview of the ALD processes investigated in this thesis is shown in Figure 3.1. In the following chapter, growth and

characterisation will be described and discussed for copper(I) oxide, copper metal and copper(I) nitride.

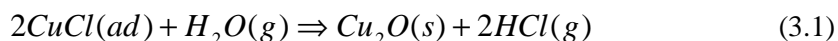
Phase →	Cu <sub>2</sub> O	Cu <sub>3</sub> N	Cu
Cu-precursor ↓			
CuCl	+ H <sub>2</sub> O	-	+ H <sub>2</sub> O/H <sub>2</sub> + H <sub>2</sub>
Cu(hfac) <sub>2</sub>	+ H <sub>2</sub> O	+ H <sub>2</sub> O/NH <sub>3</sub> + NH <sub>3</sub>	+ H <sub>2</sub> O/H <sub>2</sub> + H <sub>2</sub> O/NH <sub>3</sub>

**Figure 3.1.** Overview of the growth processes included in this thesis. The drawing shows which precursor combinations that were used to produce the different phases.

### 3.1 Copper(I) oxide

Copper oxides have many interesting properties and applications and there has been a considerable interest in vapour growth of copper oxides, ever since the discovery of the Cu-O based superconductors. Thin films of Cu<sub>2</sub>O are now studied as solar cell material [21-24], due to its low cost, non-toxicity and rather high absorption coefficient. Copper and copper oxides in general are also interesting from a catalytic point of view [25-27].

Copper(I) oxide has been grown using copper(I) chloride and water as precursors [I]. The overall reaction during the deposition process is thus thought to be an exchange reaction according to (eq. 3.1). The general growth parameters for the deposition process have been given in Table 2.1.



Previously, films of copper(I) oxide have been produced by a number of different methods. The methods range from electrochemical growth [21, 24], direct oxidation of deposited copper films [28], PVD methods [23, 29, 30] and CVD [22, 26, 31-35]. The CVD precursors used for film growth of

Cu<sub>2</sub>O were mainly metal-organic compounds and copper halides (Cu(acac)<sub>2</sub> [26, 31, 33], Cu(dpm)<sub>2</sub> [22], CuI [32] and CuCl [15]). ALD growth of copper(II) oxide (CuO) has been carried out by using CuCl and H<sub>2</sub>O/O<sub>2</sub> gas mixtures [36].

### 3.1.1 Film growth and characterisation

Films of copper(I) oxide were deposited in the temperature region from 350 to 700 °C on amorphous SiO<sub>2</sub> and single crystalline  $\alpha$ -Al<sub>2</sub>O<sub>3</sub>(102). Large differences in growth rate occurred on the two substrate surfaces, see Figure 3.2.

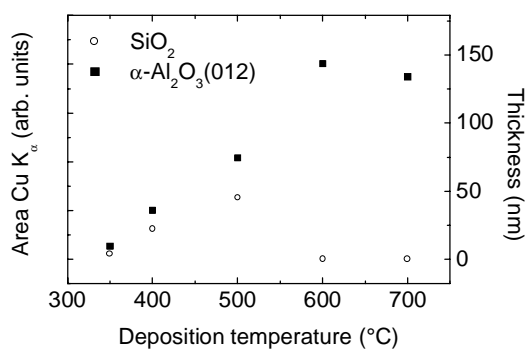


**Figure 3.2.** Deposited material as a function of deposition temperature for films grown with 1000 ALD cycles.

The growth rate was always higher on the  $\alpha$ -Al<sub>2</sub>O<sub>3</sub>(102) substrates as compared to the SiO<sub>2</sub> substrates. Films on both substrate types started to grow at 350 °C. When the deposition temperature rose to 500 °C, the growth rate increased on both substrate types, which can be explained by increased reactivity of the precursors. Furthermore, the process became substrate selective at higher growth temperatures since film growth was not possible on SiO<sub>2</sub> substrates at deposition temperatures above 600 °C. For further discussion, see paragraph 4.1.

It was found that all films contained an amount of metallic copper in addition to the desired Cu<sub>2</sub>O phase when analysed by XRD. In Figure 3.3, a representative diffractogram for a film deposited on SiO<sub>2</sub> is shown together with diffractograms from films deposited on  $\alpha$ -Al<sub>2</sub>O<sub>3</sub>(102) at different deposition temperatures.

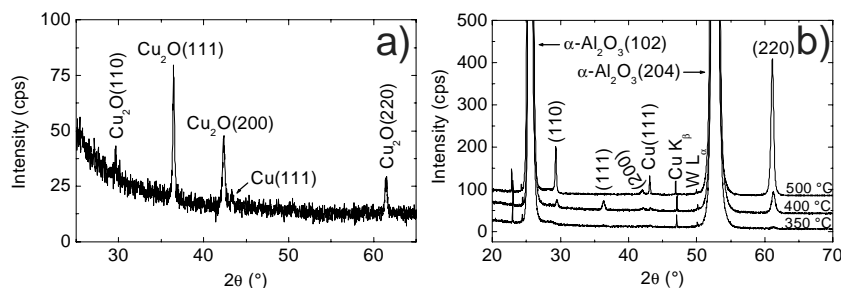


**Figure 3.3.** a) GI scan of  $\text{Cu}_2\text{O}$  deposited on  $\text{SiO}_2$  at  $500\text{ }^\circ\text{C}$  and b)  $\theta$ - $2\theta$  scans of  $\text{Cu}_2\text{O}$  deposited on  $\alpha\text{-Al}_2\text{O}_3(102)$  at different temperatures.

$\text{Cu}_2\text{O}$  deposited on  $\text{SiO}_2$  were polycrystalline and showed no texture effects. However, films deposited on the single crystalline  $\alpha\text{-Al}_2\text{O}_3(102)$  substrates were  $\{110\}$  oriented. The  $\{110\}$  preferred orientation was less pronounced at lower deposition temperatures such as  $400\text{ }^\circ\text{C}$ , whereas a strong  $\{110\}$  preferred orientation was observed at higher deposition temperatures such as  $600\text{ }^\circ\text{C}$ . Rocking curve FWHM values also indicated that the crystalline quality of the textured films improved at higher deposition temperatures. For example, the FWHM value decreased from  $0.48^\circ$  at  $400\text{ }^\circ\text{C}$  to  $0.15^\circ$  at  $600\text{ }^\circ\text{C}$ .

The presence of copper metal in the films could be related to the instability of the copper(I) chloride precursor. Several possible pathways can be thought to yield copper metal due to precursor instability; thermal decomposition of copper(I) chloride clusters upon contact with the substrate surface or by disproportionation (which is rather common for copper(I) compounds) of adsorbed precursor. The instability of the  $\text{CuCl}$  precursor was proved by pulsing with only  $\text{CuCl}$  and argon (omitting the water) at  $500\text{ }^\circ\text{C}$ . After the  $\text{CuCl}$  pulsing, a copper content was measurable by XRFS on fused silica substrates. The amount of deposited copper that related to  $\text{CuCl}$  instability corresponded to 15 % of the total copper content in a film produced in a water-based process. The instability of the  $\text{CuCl}$  precursor increased with increasing deposition temperature. Furthermore, when the films were analysed by SEM/EDS, larger grains of mainly copper metal were found on the film surface. The lateral size of the larger crystallites was about 500 nm, whereas the film in between the crystallites had a smaller average grain size, around 200-300 nm. SEM images of a film deposited on  $\alpha\text{-Al}_2\text{O}_3(102)$  are shown in Figure 3.4.

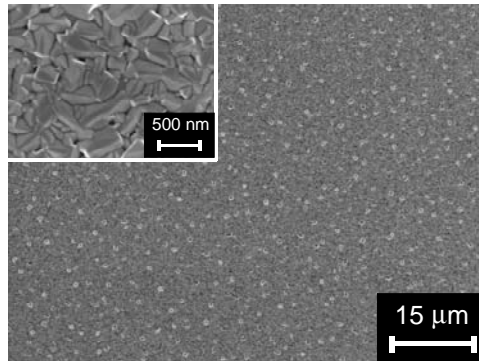


**Figure 3.4.** SEM images of a  $\text{Cu}_2\text{O}$  film deposited on  $\alpha\text{-Al}_2\text{O}_3(102)$  at  $500\text{ }^\circ\text{C}$ .

Phase pure films of  $\text{Cu}_2\text{O}$  could only be deposited by adding iodine to the water evaporator. The added iodine etched the metallic copper selectively [I].

Due to the shown precursor instability, saturation of the  $\text{CuCl}$  precursor pulse length is not to be expected (see Figure 3.5.).

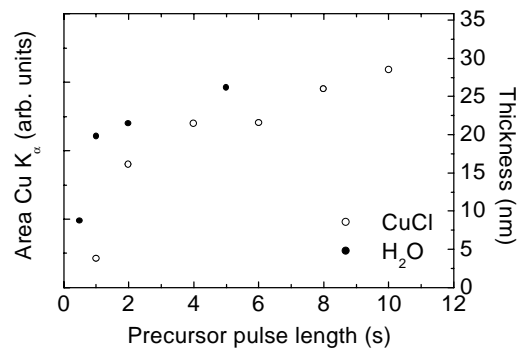


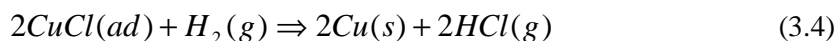
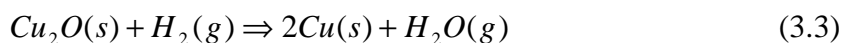
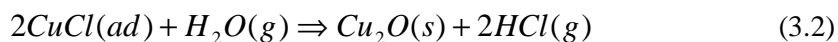
**Figure 3.5.** Deposited material as a function of precursor pulse length for films grown on  $\text{SiO}_2$  at  $400\text{ }^\circ\text{C}$  and 1000 cycles.

It can be seen that the film thickness is not leveling off when the  $\text{CuCl}$  pulse length increases. However, when the  $\text{CuCl}$  pulse length was increased from 4 to 10 s at  $400\text{ }^\circ\text{C}$ , an increase in the amount of deposited material by 25 % was observed. This indicated that the entire increase in growth rate could not be explained by  $\text{CuCl}$  instability when the 25 % value obtained at  $400\text{ }^\circ\text{C}$  was compared to the 15 %  $\text{CuCl}$  instability value obtained at  $500\text{ }^\circ\text{C}$ .

## 3.2 Copper metal

Use of copper for metallisation has obtained much interest recently, particularly in the field of microelectronics due to the good conductivity of copper. In the microelectronic applications of today, PVD and electrochemical deposition are the most commonly used methods. However, other deposition methods are investigated for deposition of copper as well. CVD is one deposition technique that has been studied extensively [18-20, 37-41]. More recently, the ALD method, known to produce films with good step coverage, has also been tested with the purpose to find a suitable process for growth of copper [42-47]. In both ALD and CVD, copper source materials can be divided into two groups; copper(I) and copper(II) type precursors. The difference between the two precursor types is their deposition pathways. For copper(II) precursors, a reducing agent is needed to grow the metallic copper. In the case of copper(I) precursors (especially for metal-organic copper(I) precursors), copper is usually grown via disproportionation reactions. Hence, the choice of reducing agent is not as crucial when films are grown from copper(I) precursors. For non-disproportionation reactions, hydrogen gas is by far the most frequently used reducing agent in the copper vapour deposition processes. The relative inertness of the hydrogen molecule leads to that the rate limiting step in copper growth processes is usually related to hydrogen activation. Therefore, deposition of copper (thermally activated) on metal surfaces has been more successful than growth on surfaces with low metal character such as oxides. Recently, plasma techniques have been coupled with the CVD/ALD methods to obtain the necessary activation energy for copper growth at lower temperatures by production of hydrogen radicals [45, 48].

Films of copper metal have been grown by two ALD processes in this work, one including water ( $\text{CuCl}/\text{H}_2\text{O}/\text{H}_2$ ) and one without water ( $\text{CuCl}/\text{H}_2$ ) [II]. Characterisation of the epitaxial films has been performed by XRD and TEM [III]. When water was included in the growth process, the copper is thought to be deposited via an oxide-forming step (see eq. 3.2 and 3.3), whereas a direct reaction between  $\text{CuCl}$  and  $\text{H}_2$  occurs in the water free process (eq. 3.4). General growth parameters for the deposition process are given in Table 2.1.



### 3.2.1 Film growth

Films of copper metal were deposited in the temperature region from 375 to 475 °C. Large differences in growth rate was observed between the two applied processes (CuCl/H<sub>2</sub>O/H<sub>2</sub> and CuCl/H<sub>2</sub>), both on the fused silica and on the alumina substrates. However, the addition of water only influenced growth rates, while the film characteristics, examined by XRD and SEM were the same. Since the quality of the deposited copper films were found to be the same with and without water included in the process, only general data for the deposition sequence including water are shown in this chapter. The differences between the two processes mainly relate to the growth mechanism, and will be discussed in chapter 4. The film thickness as a function of deposition temperature for the CuCl/H<sub>2</sub>O/H<sub>2</sub> process is shown in Figure 3.6.

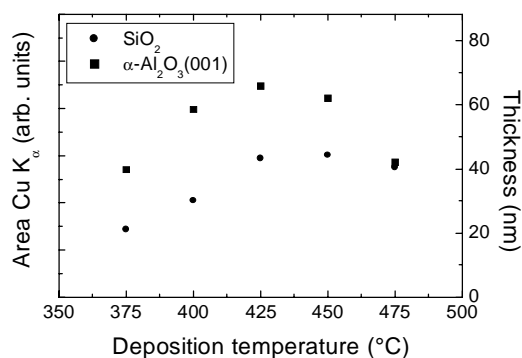


**Figure 3.6.** Deposited material as a function of deposition temperature for films grown with 500 CuCl/H<sub>2</sub>O/H<sub>2</sub> cycles.

It can be seen that the growth rate for copper grown on  $\alpha$ -Al<sub>2</sub>O<sub>3</sub>(001) was higher at all deposition temperatures, except at 475 °C. Furthermore, the growth rate increased with increasing deposition temperature up to 425 °C. At higher deposition temperatures, the growth rate started to decrease on both substrate types.

The amount of copper as a function of the number of deposition cycles for films deposited at 400 °C is shown in Figure 3.7. The growth rate of copper on  $\alpha$ -Al<sub>2</sub>O<sub>3</sub>(001) can be determined to approximately 1.2 Å/cycle, whereas the growth rate on SiO<sub>2</sub> was determined to 0.70 Å/cycle. There are many parameters that might induce differences in growth rates. For example, reactions between the precursors (CuCl, H<sub>2</sub>O and H<sub>2</sub>) and the two substrate surfaces may not be the same. This may lead to differences at the initial film growth step, when the copper grew directly on the substrates. Moreover, copper growth on copper may also be different for films grown on the two oxide substrates. For example, differences in Cu growth rates on Cu may

occur because of differences in morphology and/or crystalline order in the deposited films.

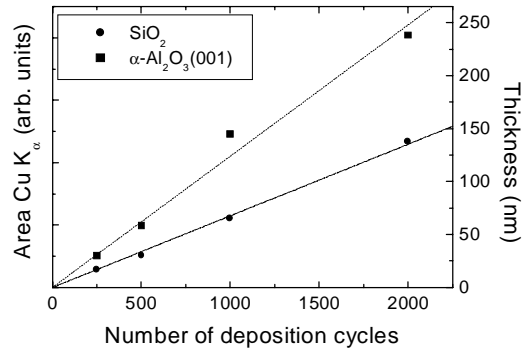


**Figure 3.7.** Deposited material as a function of the number of deposition cycles at 400 °C for films grown with the CuCl/H<sub>2</sub>O/H<sub>2</sub> process. The lines are guides for the eye.

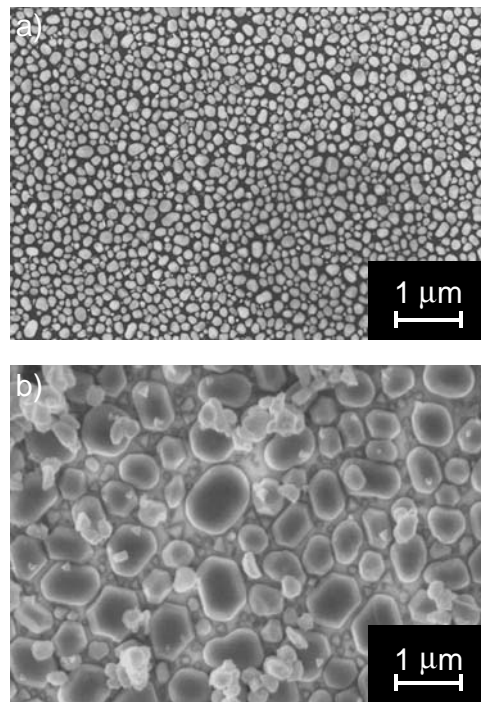


**Figure 3.8.** a) Cu deposited on SiO<sub>2</sub> at 400 °C, 500 CuCl/H<sub>2</sub>O/H<sub>2</sub> cycles and b) Cu deposited on  $\alpha$ -Al<sub>2</sub>O<sub>3</sub>(001) at 400 °C, 1000 CuCl/H<sub>2</sub>O/H<sub>2</sub> cycles.

According to the SEM and XPS investigations, the films were not completely intact. This may imply that the substrate surfaces were active during the entire deposition process, leading to the fact that several different deposition pathways may have existed simultaneously. Two SEM images are displayed in Figure 3.8, one for a film deposited on SiO<sub>2</sub> and one for a film grown on  $\alpha$ -Al<sub>2</sub>O<sub>3</sub>(001). A clear indication of the island growth behaviour is observed. Furthermore, the grain size was strongly dependent on the number of ALD cycles as well. For example, in a film deposited with 500 cycles, most grains had a size of 100 to 200 nm, whereas the grain size at 2000 cycles could be as large as 1  $\mu$ m for films deposited on SiO<sub>2</sub> substrates at 400 °C. On the  $\alpha$ -Al<sub>2</sub>O<sub>3</sub>(001) substrates, the surface was covered by both larger copper grains and some smaller ones. Some of the larger grains were rather flat as compared to the grains on the SiO<sub>2</sub> substrates. Moreover, secondary nucleation seemed to occur on some of the larger copper grains for the films deposited on  $\alpha$ -Al<sub>2</sub>O<sub>3</sub>(001). The island growth behaviour of the copper films on both substrates can probably be explained by high copper mobility, both in the copper grains and on the substrate surfaces at the rather high deposition temperatures used in this study.

### 3.2.2 Aspects of epitaxy

Films deposited on the amorphous SiO<sub>2</sub> substrates were found to be randomly oriented and polycrystalline at all deposition temperatures when characterised by XRD. For films grown on the single crystalline  $\alpha$ -Al<sub>2</sub>O<sub>3</sub>(001) substrates, the deposited copper grains showed a strong {111} orientation at all deposition temperatures. In addition to the preferred {111} orientation, a less pronounced {100} orientation was also present in the deposited films. FWHM values from  $\omega$ -scans (rocking curves) for the Cu(111) reflections were in the region from 0.044 to 0.12°, compared to FWHM values around 0.2 - 0.3° for the (200) reflections. Furthermore, the relative amount of the {100} orientation decreased when the number of ALD cycles increased. For example, the relative peak intensity, I(200)/I(111), decreased from around 1% to less than 0.05% when the number of ALD-cycles was increased from 250 to 2000. A GI-scan for a copper film deposited on SiO<sub>2</sub> is shown in Figure 3.9a, together with a  $\theta$ -2 $\theta$  and a Cu(111)  $\omega$ -scan for a film grown on  $\alpha$ -Al<sub>2</sub>O<sub>3</sub>(001), Figure 3.9b and c.

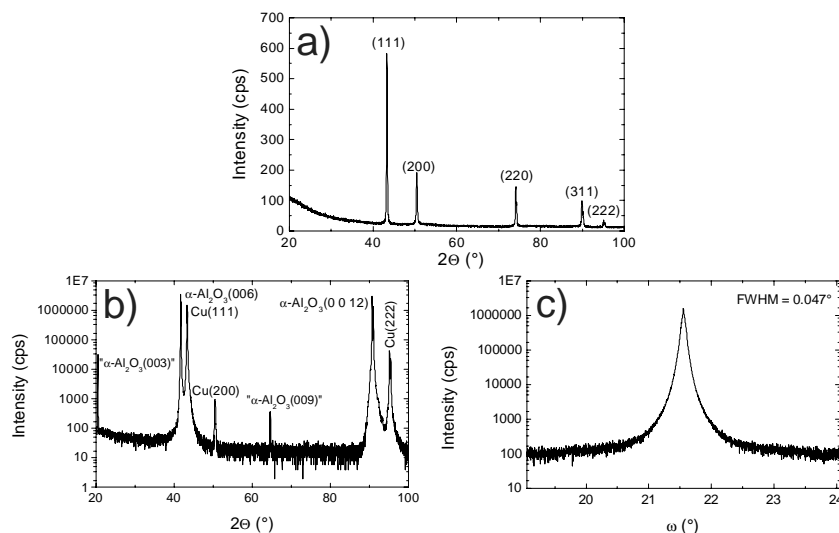


**Figure 3.9.** XRD data for copper deposited with 500 CuCl/H<sub>2</sub>O/H<sub>2</sub> cycles. a) GI scan for Cu deposited on SiO<sub>2</sub> at 400 °C, b)  $\theta$ -2 $\theta$  scan for Cu deposited on  $\alpha$ -Al<sub>2</sub>O<sub>3</sub>(001) at 425 °C and c) Cu(111)  $\omega$ -scan for the film shown in b).

The small rocking curve FWHM values indicate that copper grew epitaxially on the alumina substrates with Cu(111)// $\alpha$ -Al<sub>2</sub>O<sub>3</sub>(001). The in-planar epitaxial relationships between the copper and the substrate were calculated from a pole figure for the film and for the substrate, respectively. A Cu(200) pole figure is displayed in Figure 3.10. The six strongest peaks, at a  $\psi$ -value of 54.7°, correspond to the Cu{111} orientation. It was found that Cu(111)[1-21]// $\alpha$ -Al<sub>2</sub>O<sub>3</sub>(001)[110] (called O1) and Cu(111)[-12-1]// $\alpha$ -Al<sub>2</sub>O<sub>3</sub>(001)[110] (O1T). O1T is a twin with respect to O1, due to a packing twin ((111) and (-1-1-1)). Therefore, the six peaks originate from two 3-fold Cu(111) rotational symmetry equivalents in the Cu(200) pole figure. Furthermore, another weak (111) in-planar orientational relationship can be observed, rotated 90° with respect to O1 and O1T. The relative intensity of the 90° rotation orientation was about a few percent of O1 and O1T and decreased with increasing film thickness. A picture of the O1 and O1T in-planar orientational relations with the substrate is displayed in Figure 3.10. The axial mismatch within the corresponding substrate and film surfaces were calculated to be -6.9% along the  $\alpha$ -Al<sub>2</sub>O<sub>3</sub>[-1-10] direction and -6.8% in the  $\alpha$ -Al<sub>2</sub>O<sub>3</sub>[-110] direction, respectively. The calculated in-planar orientational relationship for the copper {111} orientation was consistent with observations in the literature, for copper grown on  $\alpha$ -Al<sub>2</sub>O<sub>3</sub>(001) by other deposition methods [49-54].

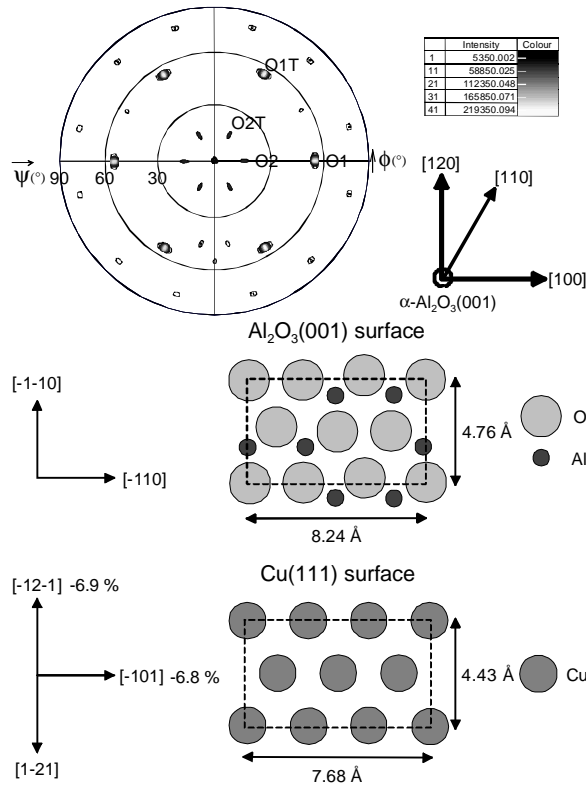


**Figure 3.10.** Top: Cu(200) pole figure for a copper film deposited with 2000 ALD-cycles at 400 °C. Bottom: Corresponding in-planar orientational relationship for the main Cu{111} orientation on the  $\alpha\text{-Al}_2\text{O}_3(001)$  substrate surface.

However, two other rings with reflections can be observed at  $\psi$ -values of 15.6 and 78.9° in the Cu(200) pole figure. The extra set of reflections cannot be related to the {111} orientation. Instead, an extra {115} orientation was found to exist in the films, where the measured  $\psi$ -values correspond to plane angles between different (115)-planes and (200)-planes. Due to its high scattering angle, the {115} orientation is not measurable in ordinary  $\theta$ -2 $\theta$  scans. To be able to measure FWHM values for the {115} orientation, asymmetrical RSM reflections can be used. Measured FWHM values were found to be around 0.15° for the {115} orientation, indicating the presence of an epitaxial relationship to the substrate for this orientation as well. The in-planar orientational relationships for the most intense peaks of the {115} orientation were calculated to  $\text{Cu}(115)[-110]//\alpha\text{-Al}_2\text{O}_3(001)[-110]$  (called O2) and  $\text{Cu}(115)[1-10]//\alpha\text{-Al}_2\text{O}_3(001)[-110]$  (called O2T). The (115) plane can also be described as a tilt of the (111) plane along the Cu[-1-12] direction in the Cu(111) surface. Finally, two smaller peaks at  $\psi = 45^\circ$  in the Cu(200) pole figure were present in the pole figure. The common feature of these minor peaks is that they do not broaden directly to or perpendicularly to the center of the pole figure. Thus, one possible explanation for these off-

center peaks is that they belong to copper grains not related directly to the substrate surface. This is not unlikely since extensive twinning in the copper grains was found in the TEM studies. Another explanation given by Knoll and Bialas [55] is that the off-center peaks emerge from steps (different crystal planes) in the  $\alpha\text{-Al}_2\text{O}_3(001)$  surface.

When analysing films by XRD, an average picture of the crystalline properties of the films is obtained. However, TEM examinations yield additional local information. As mentioned previously, copper grains can grow from a  $[-1-1-1]$  direction and thus yield O1T, which is a twin with respect to O1. Both O1 and O1T grains that grew directly from the substrate were found in an electron diffraction investigation. From literature, it is known that extensive  $\{111\}$ -twinning occurs in copper. One explanation for the twinning is that the interface energy, induced by a stacking fault in a  $\text{Cu}\langle 111 \rangle$  direction, is small, around  $0.04 \text{ J/m}^2$  [56, 57]. Thus, the copper grains can consist of several sub-grains due to  $\{111\}$ -twinning. Evidence that twinning in different  $\text{Cu}\langle 111 \rangle$  directions occurred was found, both in planes parallel to the substrate surface and in other  $\{111\}$  planes. An example of  $(111)$ -twinning in one copper grain, which consists of four layers, is shown in Figure 3.11a. From the corresponding cross-sectional Selective Area Electron Diffraction (SAED) pattern, shown in Figure 3.11b, the  $(111)$ -twin is revealed by the existence of the  $200$  and  $200_t$  reflections. Furthermore, the existence of a  $(-111)$  twin plane is shown in Figure 3.11(I). The copper grain in Figure 3.11(I) contains eight sub-grains. Four orientations in the grain were found by Convergent Beam Electron Diffraction (CBED), called a-d [Figure 3.11(II)]. The other sub-grains were found to have the same orientations as the sub-grain “a” or “c”, and are marked by (a) or (c). The CBED patterns shown in Figure 3.11(II) all have the same  $\text{Cu}[01-1]$  axis. In sub-grain “a” [and (a)], the  $\text{Cu}(111)$  plane was found to be in parallel to the substrate surface. By rotating sub-grain “a” around its  $[-111]$  axis and form a  $(-111)$  twin, sub-grain “c” is obtained. All the  $(111)$ -like sub-grains “a” and (a) and  $(-111)$  twin like sub-grains “c” and (c) have the same  $[-111]$  direction as shown in Figure 3.11(II). It should be pointed out that the  $(-5-1-1)$  plane of the  $(-111)$  twin is in parallel to the substrate surface as marked in the electron diffraction pattern c in Figure 3.11(II). Hence, all the  $(-111)$  twins contribute to the  $\{115\}$  orientation found in the  $\text{Cu}(200)$  pole figure. Moreover, no copper grains, consisting only of the  $\{115\}$  orientation, were found in the TEM characterisation (cross-section and top-view, covering more than hundred copper grains). Therefore, it is likely that  $\{115\}$  copper orientation is obtained from  $\{111\}$  twin planes (for example as a  $(-111)$  twin) rather than growing with a  $\langle 115 \rangle$  direction directly from the  $\alpha\text{-Al}_2\text{O}_3(001)$  substrate surface. Finally, sub-grain “b” can be characterised as an O1T twin and sub-grain “d” as a multi-twin of sub-grain “a” or a  $(111)$  twin of sub-grain “c”.

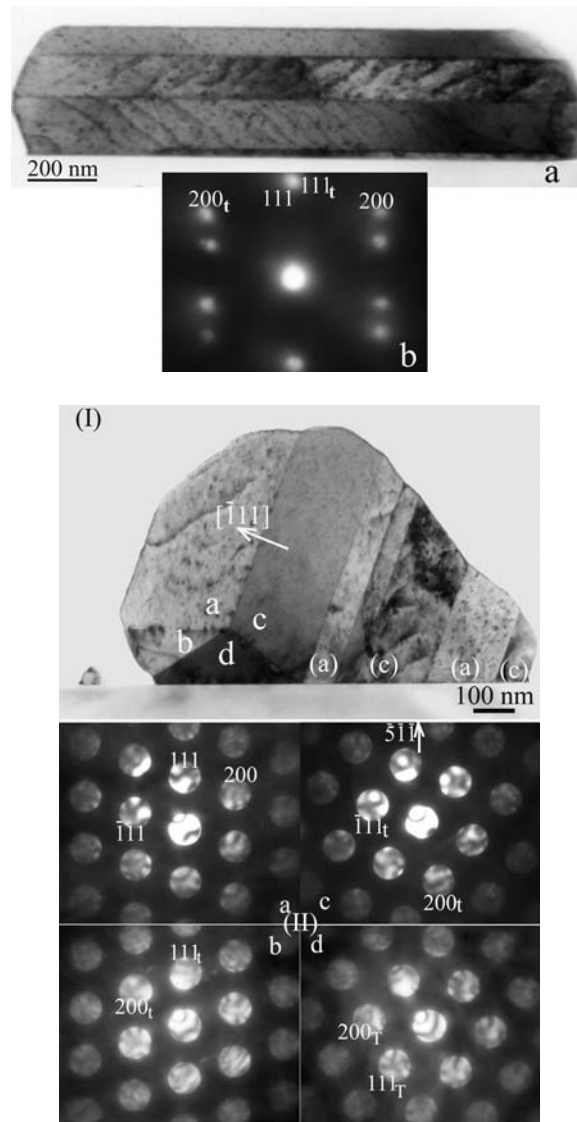


**Figure 3.11.** Top: Cross-section TEM image and SAED pattern for a copper (111)-twin. Bottom: TEM image of a copper grain consisting of eight sub-grains (I). CBED patterns from the sub-grains a-d (II).

### 3.3 Copper(I) nitride

$\text{Cu}_3\text{N}$  is a semiconductor where the band gap varies with the nitrogen content. The experimentally measured band gaps have been reported to be in the range 1.1 up to 1.8 eV [58-63].  $\text{Cu}_3\text{N}$  is a cubic compound of anti- $\text{ReO}_3$  type. The structure can be described by the nitrogen occupying the corners in the cubic unit cell, whereas the copper is situated on the cube edges. Furthermore, the  $\text{Cu}_3\text{N}$  phase is metastable, shown by a positive enthalpy of formation, 71 kJ/mol [64]. Upon heating, the copper(I) nitride decomposes thermally into metallic copper and nitrogen gas. The lowest decomposition temperature reported in the literature is around 250 °C [63]. Due to the metastability of  $\text{Cu}_3\text{N}$ , interesting metallisation applications arise. For example, dot patterns of copper, formed by argon ion etching [65] and by electron beam radiation [66], are reported as well as conducting copper lines produced by laser writing [67]. These patterns might be used for optical data storage applications [68]. Another interesting tentative large application of  $\text{Cu}_3\text{N}$  films, using the metastability, might be for metallisation in microelectronics. Copper films may be grown via the nitride and a subsequent short annealing. This procedure might offer advantages with respect to growth rate, morphology, surface roughness, grain size, adhesion and nucleation compared to of direct deposition of copper metal.

Previously, films of  $\text{Cu}_3\text{N}$  have been successfully produced by sputtering methods using copper and nitrogen as source materials [58, 60-62, 69-72]. Other  $\text{Cu}_3\text{N}$  deposition methods used are MBE [63] and ablation of copper in nitrogen ambient [73]. Since ALD is a thermally activated process, nitrogen gas can no longer be used as nitrogen source due to its inertness at lower deposition temperatures. Instead, ammonia is used as nitrogen source.  $\text{Cu}(\text{hfac})_2$  is used as copper source due to its high vapour pressure and high reactivity at lower deposition temperatures. When depositing the  $\text{Cu}_3\text{N}$  phase, two different ALD pulse sequences were applied, one including water [ $\text{Cu}(\text{hfac})_2/\text{H}_2\text{O}/\text{NH}_3$ ], and one without water [ $\text{Cu}(\text{hfac})_2/\text{NH}_3$ ] [IV]. In the growth process, where water is included, an intermediate layer of surface oxide is thought to be formed during each ALD cycle in a similar fashion as for the copper process described in section 3.2. Finally, use of  $\text{Cu}_3\text{N}$  for metallisation applications is reported in [V]. The general growth parameters for the deposition process are given in Table 2.1.

### 3.3.1 Film characterisation

Films of copper(I) nitride were deposited in the temperature region from 210 to 302 °C on SiO<sub>2</sub> and  $\alpha$ -Al<sub>2</sub>O<sub>3</sub>(001) by applying a Cu(hfac)<sub>2</sub>/H<sub>2</sub>O/NH<sub>3</sub> pulse scheme. Without water, almost no film growth occurred. No differences in film thickness occurred for films grown on the two substrate types. Therefore, only data for films deposited on SiO<sub>2</sub> are shown in the growth kinetics graphs. Film thickness as a function of deposition temperature is displayed in Figure 3.12a.

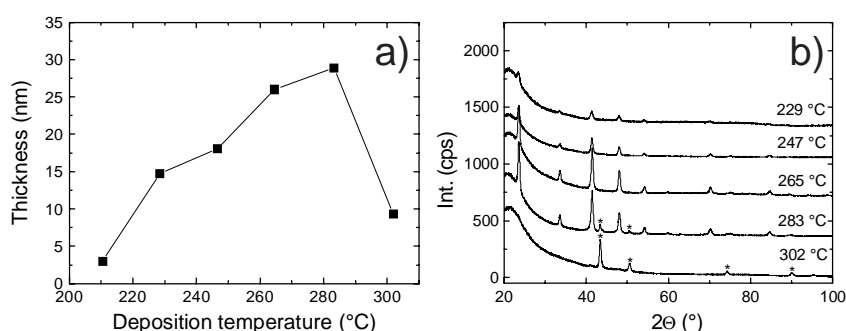


**Figure 3.12.** a) Cu<sub>3</sub>N/Cu film thickness as a function of deposition temperature for films grown with 500 cycles on SiO<sub>2</sub> and b) corresponding diffractograms. (Peaks marked with asterisks correspond to the Cu phase, whereas all unmarked peaks belong to the Cu<sub>3</sub>N phase.)

It can be seen that film growth started to occur at approximately 210 °C. After films started to grow at 210 °C, the growth rate increased with increasing deposition temperature up to approximately 280 °C. From 280 to 300 °C a steep decrease in film growth rate was observed. The corresponding diffractograms to the deposition temperature series (Figure 3.12b) show that phase pure films of Cu<sub>3</sub>N were grown at lower deposition temperatures, whereas phase mixtures of copper(I) nitride and metallic copper were obtained at 283 °C. At 302 °C, the films consisted of mainly copper metal. The presence of the copper metal phase is probably due to stability issues of the Cu<sub>3</sub>N phase. As mentioned previously, Cu<sub>3</sub>N has been reported to decompose at temperatures of 250 °C and upwards. However, the growth rate was still markedly lower at 302 °C, even if it was taken into account that the films consisted of copper instead of copper(I) nitride. (The density quotient between bulk Cu/Cu<sub>3</sub>N is ~1.5, which means that the same amount of copper atoms in a Cu<sub>3</sub>N and in a Cu film will lead to a thinner Cu film.) One explanation for the decrease in growth rate might be explained by

an increased rate of precursor desorption, which may also result in nucleation problems.

When comparing the morphology for films grown at different deposition temperatures, large differences were observed between the  $\text{Cu}_3\text{N}$  and Cu phases. SEM images for films grown on fused silica substrates at three different deposition temperatures are shown in Figure 3.13. It should be noted that film morphology was roughly the same for films deposited on  $\text{SiO}_2$  and  $\alpha\text{-Al}_2\text{O}_3(001)$  substrates.

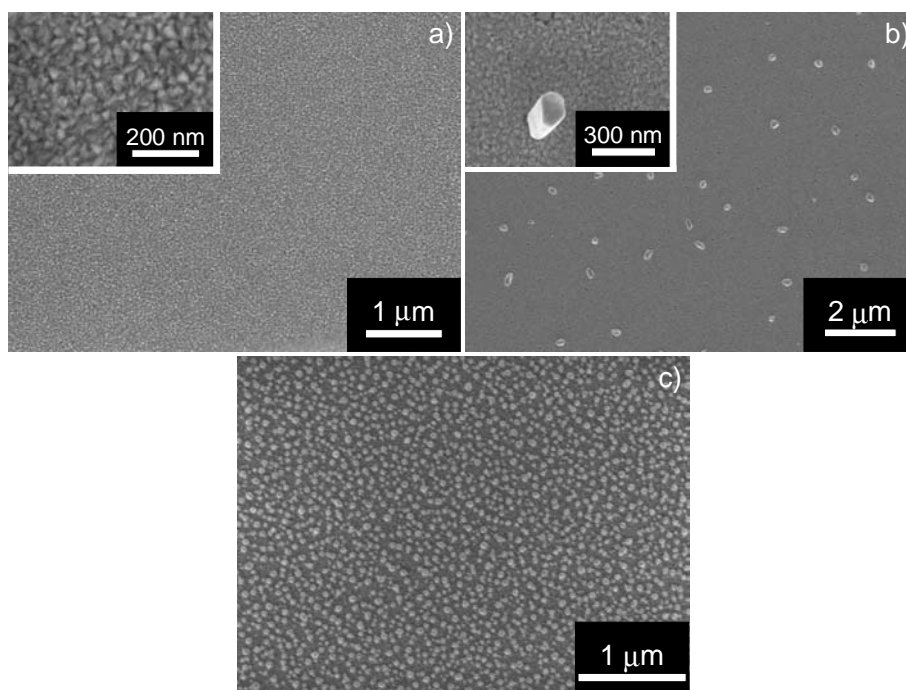


**Figure 3.13.** SEM images for Cu/ $\text{Cu}_3\text{N}$  films grown on  $\text{SiO}_2$  substrates at three different deposition temperatures. a) 1000 cycles at 247 °C, b) 500 cycles at 283 °C and c) 500 cycles at 302 °C.

At 247 °C (Figure 3.13a), homogeneous films of  $\text{Cu}_3\text{N}$  were obtained. The lateral grain size was estimated to range from 10 to 30 nm. In Figure 3.13b, SEM images for the two phase film (Cu and  $\text{Cu}_3\text{N}$ ), deposited at 283 °C, are shown. It can be seen that larger crystallites (around 100nm) have been formed on the film surface, spaced some micrometers apart. Indications of film decomposition at some areas can be observed in the regions between the larger crystallites. Due to the large diffusion rate of copper, one possible explanation is that the larger crystallites consisted mainly of copper metal, obtained by the thermal decomposition of the nitride. It should also be noted that the SEM images of the Cu/ $\text{Cu}_3\text{N}$  phase mixture show a resemblance to

the Cu/Cu<sub>2</sub>O phase mixture depicted in Figure 3.4. At the highest deposition temperature (Figure 3.13c), only larger copper grains around 50 nm existed. Furthermore, a complete surface coverage of copper could not be obtained at 302 °C, which might be due to poor nucleation conditions and/or large diffusion rates of copper on the given surfaces. However, nucleation problems existed even at lower growth temperatures such as 247 °C. Due to poor nucleation, island growth of the Cu<sub>3</sub>N films occurred. As a result, a complete surface coverage of the substrates was not obtained until a film thickness of 20 nm. At film thicknesses above 10 nm, the Cu<sub>3</sub>N grains started to coalesce and form larger connected film areas. Moreover, the grain size and roughness was approximately the same for films deposited with 500 cycles and upwards.

All films of copper(I) nitride, deposited on SiO<sub>2</sub> were polycrystalline and randomly oriented. However, Cu<sub>3</sub>N films deposited on  $\alpha$ -Al<sub>2</sub>O<sub>3</sub>(001) were epitaxial. In the epitaxial films, two film orientations, {100} and {111}, existed at different deposition temperatures. The {111} orientation was dominant (higher peak intensity and larger rocking curve FWHM value,  $\sim 2^\circ$ , than the {100} orientation) at all deposition temperatures. The amount of {100} orientation increased with decreasing deposition temperature and in films deposited with few ALD-cycles. The larger relative {100} contribution in the thinner films and the smaller rocking curve FWHM values ( $\sim 0.3^\circ$ ) indicated that the {100} orientation grew directly from the alumina substrates, whereas the {111} orientation may grow both from the substrate and on previously deposited Cu<sub>3</sub>N films. A (110) pole figure of a Cu<sub>3</sub>N film, deposited at 247 °C with 1000 cycles, is shown in Figure 3.14a. The main Cu<sub>3</sub>N{111} orientation can be seen at a  $\psi$ -value of 35.2°. Substrate peaks are also present in the Cu<sub>3</sub>N(110) pole figure (at a  $\psi$ -value of 38.2°) due to the fact that the  $\alpha$ -Al<sub>2</sub>O<sub>3</sub>(104) reflection overlaps slightly with the Cu<sub>3</sub>N(110) peak in  $2\theta$ . It was found that Cu<sub>3</sub>N(111)[1-21] $\parallel$  $\alpha$ -Al<sub>2</sub>O<sub>3</sub>(001)[110] (called O1) and Cu<sub>3</sub>N(111)[-12-1] $\parallel$  $\alpha$ -Al<sub>2</sub>O<sub>3</sub>(001)[110] (O1T). O1T is a twin with respect to O1, due to a packing twin [(111) and (-1-1-1)]. The weaker {100} orientation exists as twelve peaks at a  $\psi$ -value of 45.0°. Cu<sub>3</sub>N(200) exhibits 4-fold symmetry in a Cu<sub>3</sub>N(110) pole figure. However, there are multiple symmetry equivalents present in the  $\alpha$ -Al<sub>2</sub>O<sub>3</sub>(001) surface, spaced 30° apart. The corresponding in-planar orientational relationship was determined to Cu<sub>3</sub>N(200)[010] $\parallel$  $\alpha$ -Al<sub>2</sub>O<sub>3</sub>(001)[010]. {100} oriented epitaxial Cu<sub>3</sub>N films have earlier been deposited on a variety of substrates, Pt(100)/MgO(100) [69],  $\alpha$ -Al<sub>2</sub>O<sub>3</sub>(001) [69], MgO(100) [63] and Cu(100) [63].

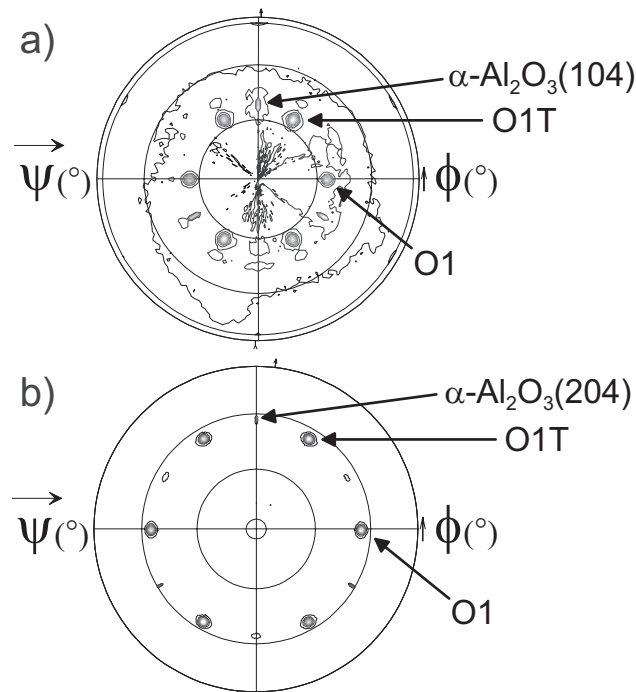


**Figure 3.14.** a)  $\text{Cu}_3\text{N}(110)$  pole figure for a  $\text{Cu}_3\text{N}$  film deposited with 1000 cycles at  $247^{\circ}\text{C}$ , b)  $\text{Cu}(200)$  pole figure for a  $\text{Cu}$  film prepared by annealing in vacuum for 15 min of the  $\text{Cu}_3\text{N}$  film used in a).

### 3.3.2 Annealing of grown $\text{Cu}_3\text{N}$ films

The metastability of the  $\text{Cu}_3\text{N}$  phase can be used to produce films of metallic copper by annealing the samples at elevated temperatures. A copper (200) pole figure (Figure 3.14b) shows that epitaxy was kept when annealing an epitaxial  $\text{Cu}_3\text{N}$  film grown on single crystalline  $\alpha\text{-Al}_2\text{O}_3(001)$ . Thus, both the films were  $\{111\}$  oriented with the same in-planar orientational relationship that was determined for the  $\text{Cu}_3\text{N}$  film described in Figure 3.14a. It should also be noticed that the  $\text{Cu}(200)$ , obtained from the annealed  $\text{Cu}_3\text{N}$  films, is similar to the  $\text{Cu}(200)$  pole figure collected for a copper film grown with the  $\text{CuCl}/\text{H}_2\text{O}/\text{H}_2$  process (see Figure 3.10). Furthermore,  $\{115\}$  orientation (probably formed due to extensive twinning in different  $\text{Cu}\langle 111\rangle$  directions) is also present in the annealed copper film. The  $\{115\}$  orientation corresponding peaks were weak and are not shown in the pole figure. It was found that both annealing temperature and annealing time played an important role for the phase transition. For example, at a temperature of  $330^{\circ}\text{C}$ , annealing times around two hours was needed to convert the copper(I) nitride into metallic copper, whereas 15 min was more than enough at an annealing temperature of  $450^{\circ}\text{C}$ . Comparing resistivity values for  $\text{Cu}_3\text{N}$

films deposited on SiO<sub>2</sub> and annealed at the two temperatures, the resistivity was around 30% lower for the films annealed at 450 °C. Thus, a higher annealing temperature during a shorter period of time was more favourable in terms of film resistivity. One possible explanation is that the film morphology became rougher during a longer annealing time due to higher copper diffusion rates (both on the substrates and in copper) even at lower temperatures such as 330 °C. In Figure 3.15, film thickness as a function of the number of deposition cycles and resistivity values are shown for Cu<sub>3</sub>N films deposited on SiO<sub>2</sub>. The films were annealed in vacuum for 15 min at 450 °C.

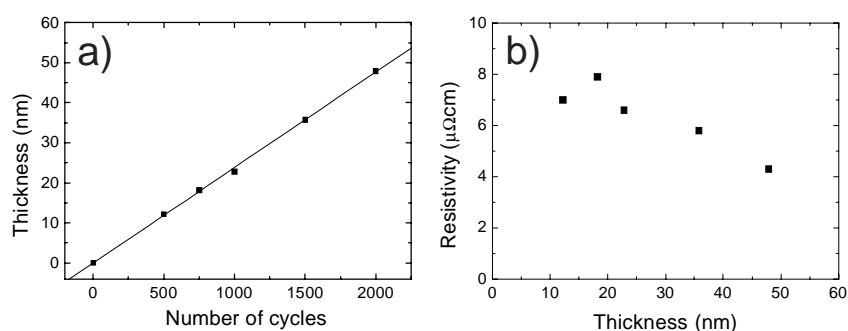


**Figure 3.15.** a) Film thickness for annealed Cu<sub>3</sub>N films grown at 247 °C on SiO<sub>2</sub> and b) resistivity as a function of copper film thickness. The copper films were prepared by annealing Cu<sub>3</sub>N films in vacuum for 15 min.

Because of the island growth during the initial deposition process, resistivity values for the copper films started to be measurable at thicknesses of approximately 10 nm. A 10 nm copper film corresponded to a 15 nm thick as deposited Cu<sub>3</sub>N film. The resistivity values decreased from 7-8 to 4 μΩcm when the film thickness increased from 10 to 50 nm. The film resistivity was still quite high, which might be due to impurities or rough film morphology. In a diffractogram from a film annealed for 15 min in vacuum, small peaks, corresponding to the Cu<sub>2</sub>O phase, could be identified. The presence of oxygen originates from the Cu<sub>3</sub>N growth process [IV], where the oxygen content was measured to 3.7 at% by XPS. However, the oxygen content could be lowered by annealing the films in hydrogen after the first anneal in vacuum. It was found that oxygen removal did not lower film resistivity values significantly. On the other hand, formation of pinholes occurred in the annealed films. SEM images from a film deposited with 1500 cycles and annealed for 15 min in vacuum, followed by a 15 min anneal in hydrogen are displayed in Figure 3.16. It can be seen that major parts of the film surface is rather uniform. The pinholes were most likely formed during the annealing

process since the copper(I) nitride films completely covered the substrate surface. However, it is probably possible to lower the resistivity values further by optimising the annealing procedure.

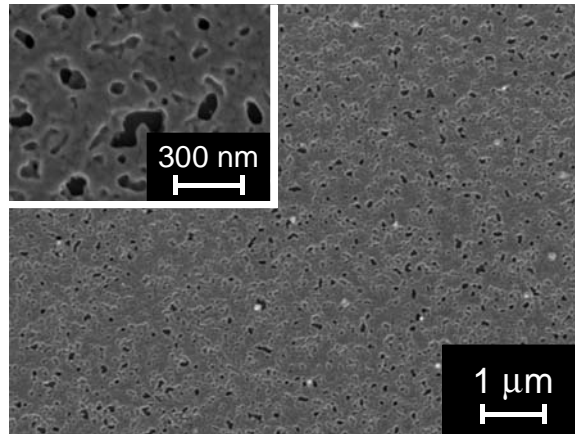


**Figure 3.16.** Copper film produced by annealing a  $\text{Cu}_3\text{N}$  film grown by 1500 cycles at  $247\text{ }^\circ\text{C}$ . The film was annealed in vacuum for 15 min at  $450\text{ }^\circ\text{C}$ , followed by 15 min anneal in hydrogen atmosphere at  $450\text{ }^\circ\text{C}$ .

## 4 Growth mechanisms

Film growth by chemical methods such as CVD and ALD occur via numerous deposition pathways. The growth mechanism is generally difficult to determine exactly. It is also possible that several competing growth mechanisms exist simultaneously in a film deposition process. In a pulsed deposition process such as ALD, the precursors are separated by pulses of inert carrier gas. After pulsing with a precursor and a subsequent purging pulse, the precursor covers the film/substrate surface (assuming that the precursor adsorb and that the rate of desorption is not too large). In a standard ALD process, two precursors are generally used. Hence, evolution of reaction products may occur during two steps in the ALD pulse sequence, where one precursor reacts with a surface termination of the other precursor during the first precursor pulse. In the second precursor pulse, the opposite occurs. Examples of film growth in more than one step during each ALD cycle have been given for growth of binary metal oxides, where water was used as oxygen containing precursor [73-76]. In water based oxide processes, the presence of surface hydroxyl groups are important because they may remain on many oxide surfaces, even at higher temperatures. Furthermore, the growth mechanism may differ between the initial and final stages of the deposition process. The difference occurs because of the fact that film growth on a substrate surface may not follow the same deposition pathway as film growth after a completely intact film has been formed on the substrate surface.

### 4.1 Copper(I) oxide

#### 4.1.1 Experimental

The films were grown by applying copper(I) chloride and water as source materials. A uniform  $\text{Cu}_2\text{O}$  thickness profile could not be obtained in the deposition zone. It was found that films grown in the downstream direction of the reactor were markedly thinner than films grown on substrates placed in positions closer to the precursor inlet [I]. The non-uniform thickness profile may be explained by the fact that hydrogen chloride is the most probable reaction product in the process, leading to etching of the newly

formed film. General film growth characteristics for the copper(I) oxide deposition process have been described briefly in paragraph 3.1. It was found that large differences in film growth rate occurred on the two substrate types,  $\text{SiO}_2$  and  $\alpha\text{-Al}_2\text{O}_3(102)$  (see Figure 3.2). From literature, water is known to adsorb and form more or less strong chemical bonds on a manifold of different surfaces, particularly oxides. For example, strong bonds are created on modifications of aluminium and silicon oxides [78]. Furthermore, indications that the majority of the chemisorbed hydroxyl groups desorb at a higher temperature on aluminium oxide than on silicon oxide exist [78]. A tentative deposition pathway, describing the surface termination (with respect to  $\text{CuCl}$  and  $\text{OH}$ -groups) during the steps in an ALD-cycle, is shown in Figure 4.1.

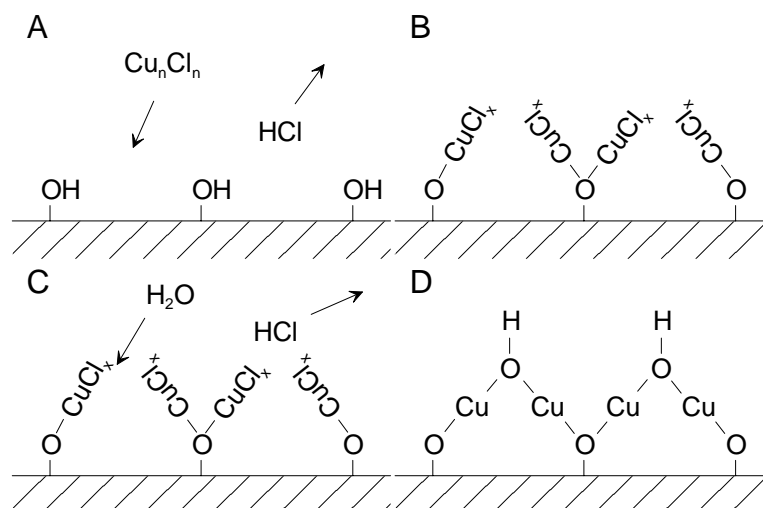


**Figure 4.1.** Tentative deposition pathway. Supply of  $\text{CuCl}$  in A and of water in C. Ar purging in B and D.

The presence of adsorbed hydroxyl groups on the substrate surfaces indicated that  $\text{HCl}$  was produced, at least initially, in two steps during each ALD-cycle at the lower deposition temperatures. At the first step, water is supplied to a surface terminated by  $\text{CuCl}$ . After the water pulse, the surface is terminated by hydroxyl groups, desorbing at some given rate. When pulsing again with  $\text{CuCl}$ , film growth occurred because hydroxyl groups were already present at the surface. Thus, at lower deposition temperatures, one explanation for the difference in  $\text{Cu}_2\text{O}$  growth rate on the two oxide substrates may be due to different nucleation properties caused by the fact that different amounts of hydroxyl groups were present on the two oxide surfaces. The difference in growth behaviour at higher temperatures between the two substrate types might be due to low sticking probability of the  $\text{CuCl}$  precursor on the amorphous  $\text{SiO}_2$  and/or because the amount of adsorbed

hydroxyl groups on the  $\text{SiO}_2$  surface was low, which may cause nucleation problems. At even higher deposition temperatures such as  $700\text{ }^\circ\text{C}$ , a decrease in the growth rate on  $\alpha\text{-Al}_2\text{O}_3(102)$  could be observed as well. Furthermore, differences in growth mechanism for  $\text{Cu}_2\text{O}$  growth on  $\text{Cu}_2\text{O}$  may also occur, for example, because the two films show different resistance against reaction with  $\text{HCl}$  due to their different orientation (crystallinity).

#### 4.1.2 DFT calculations

The copper(I) oxide growth process has been studied by ab-initio DFT, where the calculations treat  $\text{Cu}_2\text{O}$  film growth on two different  $\text{Cu}_2\text{O}$  surfaces, (111) and (110). The (111) and (110) surfaces were prepared by performing geometry optimisations on  $\text{Cu}_2\text{O}$  slabs with increasing thickness until atomic distances in the interior of the slabs and surface energies converged. No larger surface relaxation was observed for the (111) surface, whereas a downward movement for the copper surface atoms by  $0.6\text{ \AA}$  could be seen for the (110) surface. Models of relaxed and unrelaxed surface slabs are shown in Figure 4.2.

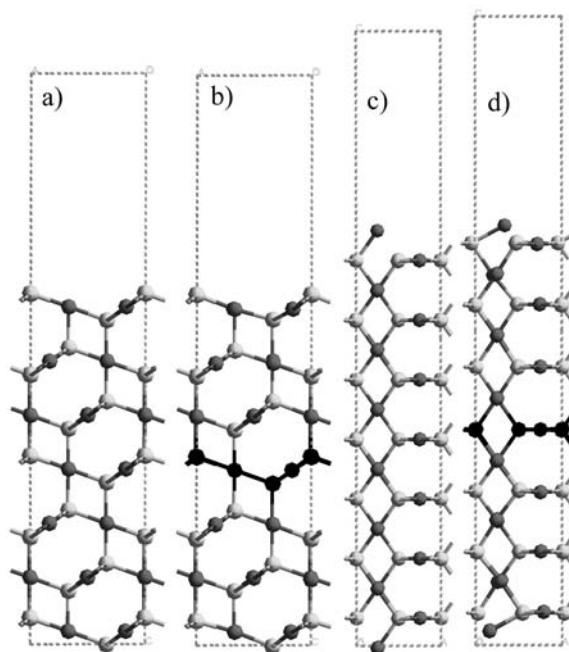


**Figure 4.2.** Relaxed and unrelaxed 7-layer models of  $\text{Cu}_2\text{O}(111)$  and (110). Light grey depicts oxygen, whereas dark grey indicates copper, and black is used for atoms in fixed positions during the surface geometry optimisations. a) Unrelaxed (111) surface, b) relaxed (111) surface, c) unrelaxed (110) surface and d) relaxed (110) surface.

The relative inertness of the Cu<sub>2</sub>O(111) surface could be seen by comparing surface energies for the slabs in Figure 4.2. It was found that the surface energy was 0.8 J/m<sup>2</sup> for the relaxed (111) slab, as compared to 0.9 J/m<sup>2</sup> for the unrelaxed (111) slab. The larger surface relaxation for the Cu<sub>2</sub>O(110) surface was also noticed by the fact that the surface energy decreased from 1.4 to 1.0 J/m<sup>2</sup> for the unrelaxed and relaxed (110) slabs, respectively. However, the two surfaces displayed similar surface energies after relaxation, indicating that the difference in surface stability was small. For the adsorption energy calculations, the top layers from the relaxed (111) and (110) slabs were used. The computational framework and level of theory used in this study have been described in section 2.2. For further information regarding the test calculations and preparation of the Cu<sub>2</sub>O surface models, see [VI].

The different surface reactions in the tentative deposition pathway are given in Figure 4.1 and were used as a starting point for the theoretical calculations. Thus, reactions where a CuCl molecule interacts from the gas phase with adsorbed hydroxyl groups (Figure 4.1a) were modelled and compared to reactions where gaseous H<sub>2</sub>O interacts with adsorbed CuCl (Fig 4.1c). The reaction pathway studies were performed on (111) and (110) surfaces of Cu<sub>2</sub>O, respectively. Furthermore, a third possibility, co-adsorption of the two precursors was evaluated for the Cu<sub>2</sub>O(111) surface. For simplicity, CuCl was treated as a monomer in the gas phase even though it exists mainly as tri- and tetramers at most of the deposition temperatures used in the experimental study. The total energy for the overall reaction was calculated according to equation 2.1. Calculated reaction energies for film growth on the (111) surface of Cu<sub>2</sub>O are given in Table 4.1. Reactions corresponding (111) surface models are displayed in Figure 4.3.

**Table 4.1.** Reaction energies for some different reaction pathways on Cu<sub>2</sub>O(111).

Reaction pathway	Surface reaction	Reaction energy (eV)
Fig. 4.3a	CuCl on Cu <sub>2</sub> O(111)	1.7
Fig. 4.3a	H <sub>2</sub> O on Cu <sub>2</sub> O(111)	0.54
Fig. 4.3b	H <sub>2</sub> O on adsorbed CuCl	0.35
Fig. 4.3c	CuCl on adsorbed H <sub>2</sub> O	1.5
Fig. 4.3d	CuCl on adsorbed H <sub>2</sub> O	0.41
Fig. 4.3.e	Co-adsorption of CuCl and H <sub>2</sub> O	-1.4

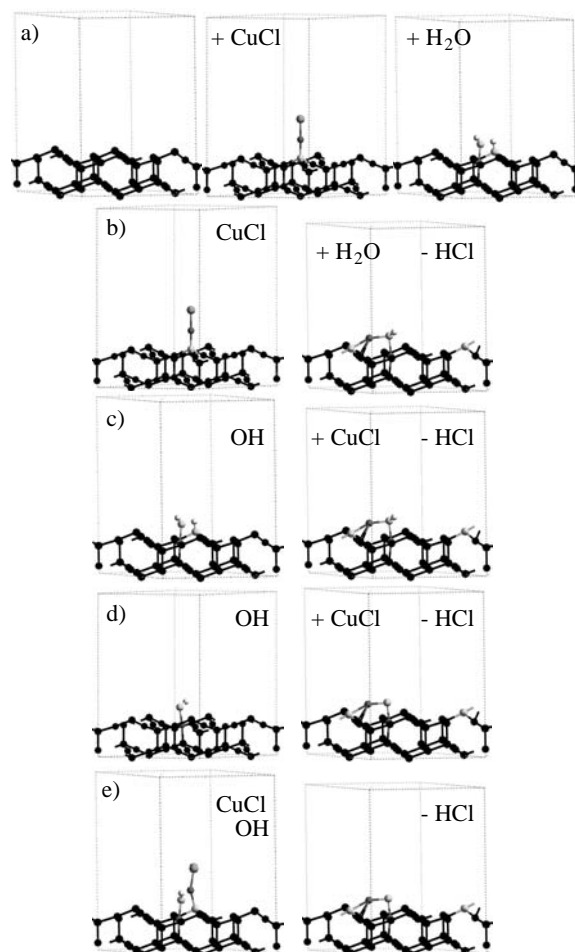


**Figure 4.3.** Surface reactions between CuCl and H<sub>2</sub>O on the (111) surface of Cu<sub>2</sub>O. a) Adsorption of CuCl and H<sub>2</sub>O, b) H<sub>2</sub>O reacts from the gas phase with adsorbed CuCl, c) CuCl reacts from the gas phase with two adsorbed hydroxyl groups, d) CuCl reacts from the gas phase with one adsorbed hydroxyl groups and e) surface reaction between an adsorbed hydroxyl group and CuCl molecule. Black depicts fixed atoms during the geometry optimisations, lightest grey shows oxygen, intermediate grey is chlorine, darkest grey indicates copper, whereas hydrogen atoms are white.

On the Cu<sub>2</sub>O(111) surface, it was found that both adsorption of CuCl and dissociative adsorption of H<sub>2</sub>O on a clean (111) surface were advantageous from an energetical viewpoint. The difference in adsorption energy was quite large between the species, over 1 eV, with adsorption of CuCl on the (111) surface being more advantageous. However, the DFT calculations were performed at 0 K. Therefore, a question mark arises, especially regarding the surface stability of the hydroxyl adsorbates at the deposition temperatures used during the ALD film growth. Experimentally, no hydroxyl groups are

expected to exist on Cu<sub>2</sub>O at higher deposition temperatures such as 600 °C. At these temperatures even strongly adsorbed hydroxyl groups on the substrates have been measured to start to desorb [78]. From an adsorption study of water on a single crystalline Cu<sub>2</sub>O(100) surface, chemisorbed hydroxyl groups were measured to desorb by formation of water at temperatures up to 250 °C when the sample was heated by 2 °C/s [79]. However, the surface coverage of adsorbed species is not only dependent on temperature but on a time factor as well. It is reasonable to suspect that the hydroxyl coverage on the film surface is maintained as long as a H<sub>2</sub>O pulse is applied in ALD. Thereafter, the coverage is probably a function of temperature and duration of purge pulse, until pulsing with CuCl occurs. Since the deposited films are far from being well-defined single crystals some hydroxyl groups may be present on the Cu<sub>2</sub>O surface at the lower deposition temperatures used in the Cu<sub>2</sub>O growth study. In Table 4.1, it can be seen that film growth via co-adsorption (Figure 4.3e) of water and CuCl is by far the less advantageous deposition pathway (-1.4 eV) on the (111) surface. Two reactions from the gas phase, on one CuCl (Figure 4.3b) and one hydroxyl (Figure 4.3d) terminated surface were around 1.8 eV more beneficial than the co-adsorption reaction. The most favourable deposition pathway on the Cu<sub>2</sub>O(111) surface was a CuCl molecule reacting with two hydroxyl groups (Figure 4.3c), with an overall reaction energy of 1.5 eV.

A similar trend in surface reaction energies was observed when corresponding models were geometry optimised on the (110) surface of Cu<sub>2</sub>O. [The co-adsorption reaction pathway was not investigated for the (110) surface since the reaction pathway seemed unlikely to occur on the (111) surface.] Calculated reaction energies for the different deposition pathways on Cu<sub>2</sub>O(110) are listed in Table 4.2, whereas corresponding surface models are displayed in Figure 4.4.

**Table 4.2.** Reaction energies for some different reaction pathways on Cu<sub>2</sub>O(110).

Reaction pathway	Surface reaction	Reaction energy (eV)
Fig. 4.4a	CuCl on Cu <sub>2</sub> O(110)	2.2
Fig. 4.4a	H <sub>2</sub> O on Cu <sub>2</sub> O(110)	0.40
Fig. 4.4b	H <sub>2</sub> O on adsorbed CuCl	-0.15
Fig. 4.4c	CuCl on adsorbed H <sub>2</sub> O	1.7
Fig. 4.4d	CuCl on adsorbed H <sub>2</sub> O	0.18
Fig. 4.4.e	CuCl on adsorbed H <sub>2</sub> O	1.3

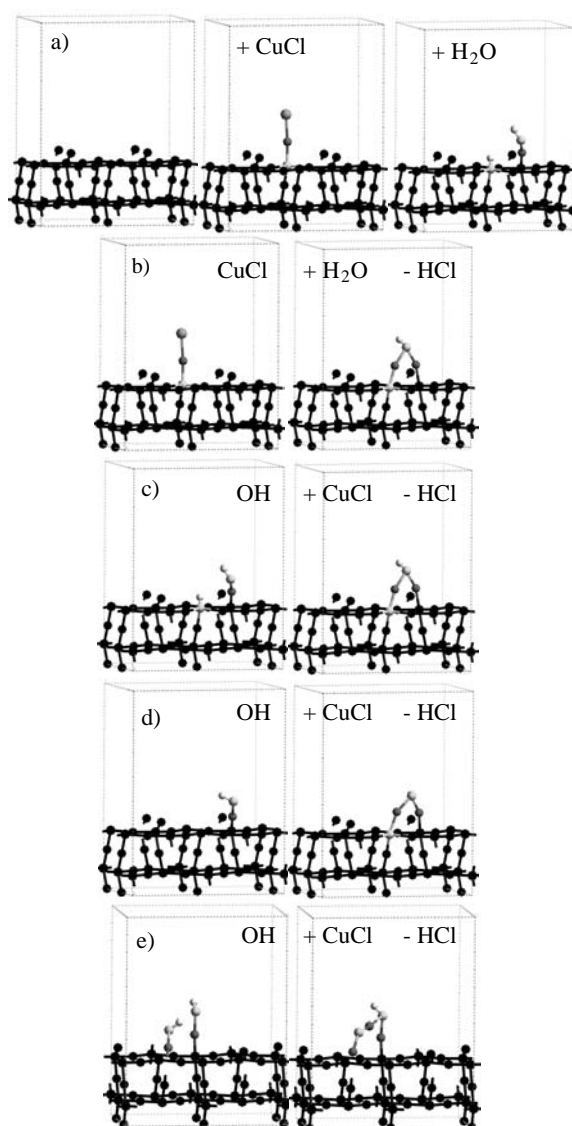


**Figure 4.4.** Surface reactions between CuCl and H<sub>2</sub>O on the (110) surface of Cu<sub>2</sub>O. a) Adsorption of CuCl and H<sub>2</sub>O, b) H<sub>2</sub>O reacts from the gas phase with adsorbed CuCl, c) CuCl reacts from the gas phase with two adsorbed hydroxyl groups, d) CuCl reacts from the gas phase with one adsorbed hydroxyl groups and e) CuCl reacts from the gas phase with two adsorbed hydroxyl groups. Black depicts fixed atoms during the geometry optimisations, lightest grey shows oxygen, intermediate grey is chlorine, darkest grey indicates copper, whereas hydrogen atoms are white.

On the (110) surface, the surface reactions (Figure 4.4c and e) where CuCl reacted from the gas phase with two adsorbed hydroxyl groups were found to be the most energetically favourable pathways. The reaction pathway where water reacted with adsorbed CuCl (Figure 4.4b) was more than 1 eV

less favourable than the calculated reaction pathways in Figure 4.4c and e. Furthermore, a large difference in adsorption energies between CuCl and H<sub>2</sub>O was observed on Cu<sub>2</sub>O(110), which is consistent with the results calculated for the Cu<sub>2</sub>O(111) surface. In conclusion, if hydroxyl groups exist on the Cu<sub>2</sub>O surface at the deposition temperatures used in the ALD study, reactions between gaseous CuCl and adsorbed hydroxyl groups were found to be the most favourable reaction pathways in the theoretical calculations. (Under the assumption that no larger barriers of adsorption are present for the proposed deposition pathways.) The amount of hydroxyl groups on the surfaces seemed to influence the process as well, where more surface hydroxyl groups led to a more advantageous reaction pathway. It should also be noted that a reaction pathway where the number of CuCl adsorbates were increased on the Cu<sub>2</sub>O(111) surface was tested on a smaller surface slab model. On the contrary to the hydroxyl coverage, the total reaction energy was less favourable for a reaction between a water molecule and two CuCl adsorbates than between a water molecule and one CuCl adsorbate. Finally, one alternative explanation for the low growth rate at the lowest deposition temperatures such as 350 °C may be due to the strong bonds formed between the CuCl precursor and the Cu<sub>2</sub>O surface. Hence, without enough thermal activation, the Cu<sub>2</sub>O surfaces may have been rather inert due to an adsorbed layer of CuCl molecules.

## 4.2 The effect and use of intermediate water pulses

The effect of adding water as an intermediate reaction step in the ALD film growth processes was investigated for deposition of copper and copper(I) nitride thin films. The general deposition characteristics for deposition of metallic copper, using a CuCl/H<sub>2</sub>O/H<sub>2</sub> pulse sequence were described in section 3.2, whereas growth of Cu<sub>3</sub>N from Cu(hfac)<sub>2</sub>/H<sub>2</sub>O/NH<sub>3</sub> was treated in section 3.3.

### 4.2.1 The CuCl/H<sub>2</sub>O/H<sub>2</sub> process

In Figure 3.6, film growth rate as a function of deposition temperature for the CuCl/H<sub>2</sub>O/H<sub>2</sub> process was compared for the two substrate types. It was found that growth rates were higher on  $\alpha$ -Al<sub>2</sub>O<sub>3</sub>(001) than on SiO<sub>2</sub>. Moreover, large differences in film growth rate were observed when the water-based process (CuCl/H<sub>2</sub>O/H<sub>2</sub>) was compared to a water-free CuCl/H<sub>2</sub> process on the two substrate types (Figure 4.5). It can be seen that for films grown on SiO<sub>2</sub>, the addition of water does not increase the growth rate. In fact, films deposited with water included in the ALD-cycle were thinner than the films made without water for all deposition temperatures except for 375 °C.

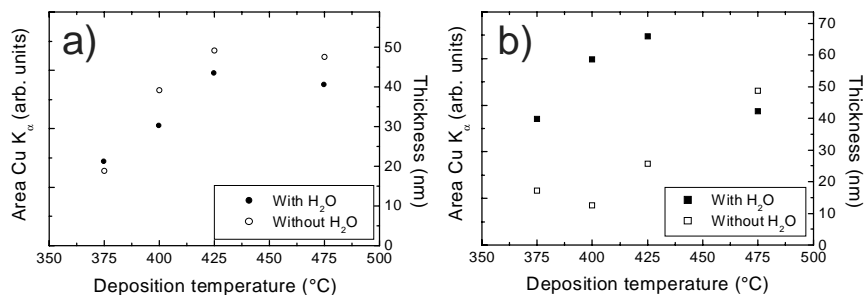


**Figure 4.5.** Copper film thickness as a function of deposition temperature for films grown with 500 CuCl/H<sub>2</sub>O/H<sub>2</sub> or CuCl/H<sub>2</sub> cycles. a) SiO<sub>2</sub> substrates and b) α-Al<sub>2</sub>O<sub>3</sub>(001) substrates.

In contrast, the addition of water increased the growth rate drastically for films deposited on α-Al<sub>2</sub>O<sub>3</sub>(001) substrates, except at the highest deposition temperature, 475 °C. One explanation for the different growth rates in the water-based process on alumina and fused silica, may be due to the surface coverage of hydroxyl groups as mentioned for the copper(I) oxide process in section 4.1. Hence, if more hydroxyl groups were present on α-Al<sub>2</sub>O<sub>3</sub>(001) than on the SiO<sub>2</sub> substrates after the water pulse, that may have led to differences in copper growth rate during the CuCl pulse. (Assuming that the hydrogen pulsing does not remove all hydroxyl groups on the substrate surfaces.) Also, a complete metal coverage of the substrate surfaces was never obtained in this work (Figure 3.8). This meant that the substrates could be active and influence film growth behaviour during the entire deposition process. Hence, the contribution to the film growth by different mechanisms may vary during the process as the surface coverage is changing. Moreover, initial film nucleation may be more advantageous with many hydroxyl groups on the substrate surfaces.

When water was excluded from the growth processes, film thicknesses on the two substrate types were within 2 nm from each other for copper grown at 375 and 475 °C. In the middle of the temperature range, higher growth rates were observed on the SiO<sub>2</sub> substrates for the CuCl/H<sub>2</sub> process. This indicates that the water-free film deposition process seemed to be more difficult to activate on the alumina substrates than on the SiO<sub>2</sub> substrates. An additional feature that could have influenced film growth throughout the whole deposition process was catalysis by the substrate. For example, the two substrate types alumina and silica might react in a different way against precursors like copper(I) chloride.

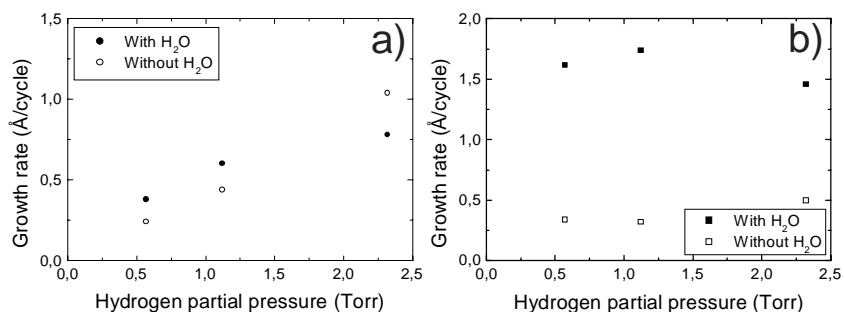


**Figure 4.6.** Growth rate as a function of hydrogen partial pressure for films deposited with CuCl/H<sub>2</sub>O/H<sub>2</sub> or CuCl/H<sub>2</sub> cycles at 425 °C. a) SiO<sub>2</sub> substrates and b) α-Al<sub>2</sub>O<sub>3</sub>(001) substrates.

The effect of hydrogen partial pressure on the deposition processes is shown in Figure 4.6. A stronger dependence on the amount of hydrogen is displayed for both growth processes on SiO<sub>2</sub> substrates than on the α-Al<sub>2</sub>O<sub>3</sub>(001) substrates. On fused silica, partial pressures lower than 2.3 Torr led to a higher growth rate for the water-based process than for the water-free process. Thus, one can speculate that the extra water step was unnecessary at higher hydrogen partial pressures, since the hydrogen activity was large enough to effectively react with the CuCl precursor. The lower growth rate (in the water-based process) may stem from the fact that a significant number of hydroxyl groups were not present on the surface. Therefore, the growth rate may have been lower because a reaction between CuCl and H<sub>2</sub>O produces an oxide over layer. The produced oxide is susceptible to HCl etching, whereas copper that is formed via a reaction between CuCl and H<sub>2</sub> in the water-free process is not. However, films deposited on the alumina substrates indicated a smaller variation in growth rate as a function of hydrogen partial pressure. This indicated that the hydrogen in the last reaction step in the CuCl/H<sub>2</sub>O/H<sub>2</sub> process was easier to activate than the hydrogen applied directly to the CuCl precursor. Without water, low growth rates were obtained at all hydrogen partial pressures.

#### 4.2.2 The Cu(hfac)<sub>2</sub>/H<sub>2</sub>O/NH<sub>3</sub> process

In the copper(I) nitride process, the addition of water to the pulse sequence was crucial. On the contrary to the copper growth process (CuCl/H<sub>2</sub>O/H<sub>2</sub>), it was found that almost no film deposition occurred without water [Cu(hfac)<sub>2</sub>/NH<sub>3</sub>] on the substrates, α-Al<sub>2</sub>O<sub>3</sub>(001) and SiO<sub>2</sub>. Hence, it is probable that hydroxyl groups were needed on the substrate surfaces to initiate the film growth, so that the Cu(hfac)<sub>2</sub> precursor was able to react

with the adsorbed hydroxyl groups from the gas phase. Thus, one explanation for the lack of film deposition in the water-free process may be due to difficulties in activating the  $\text{Cu}(\text{hfac})_2$  precursor. Furthermore no difference in film growth rate was observed on the two substrate types, which is in contradiction to observations from the  $\text{CuCl}/\text{H}_2\text{O}/\text{H}_2$  process, where film growth was found to be larger on alumina in the water-based process. One explanation to the similarity in film growth rate on both substrate types in the  $\text{Cu}(\text{hfac})_2$  based process may be due to lower deposition temperatures, less than  $300\text{ }^\circ\text{C}$ . Thus in the  $\text{Cu}_3\text{N}$  process, the coverage of surface hydroxyl groups may have been large on  $\text{SiO}_2$  as well as on  $\alpha\text{-Al}_2\text{O}_3(001)$ . However, the effect on film growth rate by adding water to the ALD cycle was only found to be significant during the initial stages of the film deposition. That is, growth of  $\text{Cu}_3\text{N}$  on top of  $\text{Cu}_3\text{N}$  seemed to be equally fast with or without the addition of water [IV]. The growth rates on  $\text{Cu}_3\text{N}$  with or without water were also verified by QCM.

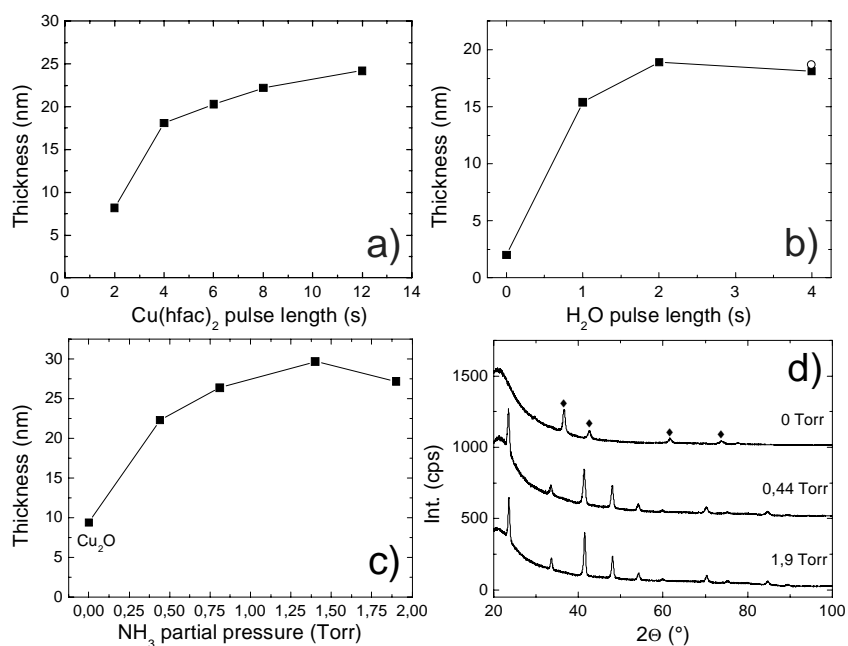


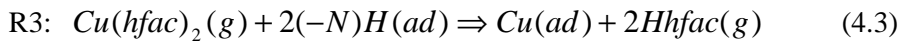
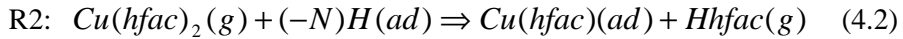
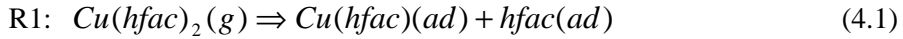
**Figure 4.7.** Film thickness as a function of precursor pulse length/partial pressure for films grown on  $\text{SiO}_2$  at  $247\text{ }^\circ\text{C}$ . a)  $\text{Cu}(\text{hfac})_2$  pulse length for film grown with 500 cycles, b)  $\text{H}_2\text{O}$  pulse length for films grown with 500 cycles (The filled squares correspond to a water dose of 2,4 mg/pulse and the open circle to a 4,1 mg/pulse water dose.), c)  $\text{NH}_3$  partial pressure for films grown with 750 cycles and d) GI-scans for some films grown with different  $\text{NH}_3$  partial pressures, where peaks marked with filled diamonds correspond to the  $\text{Cu}_2\text{O}$  phase, while all unmarked peaks belong to the  $\text{Cu}_3\text{N}$  phase.

Growth kinetics data for the  $\text{Cu}_3\text{N}$  process are displayed in Figure 4.7. It can be seen that a reasonable saturation was achieved for the water pulse (Figure 4.7b) but not for the  $\text{Cu}(\text{hfac})_2$  pulse length (Figure 4.7a). Different growth mechanisms are discussed further in conjunction to a QCM investigation of the  $\text{Cu}_3\text{N}$  process later on in this section. After the  $\text{Cu}(\text{hfac})_2$  and water pulsing, ammonia was used as a third precursor to remove the oxide overlayer thought to have been formed during the water pulse. During the water pulse it is probable that any adsorbed hfac ligands desorb as  $\text{Hhfac}$  after reacting with the water precursor. The effect of varying the ammonia partial pressure between 0 and 2 Torr was studied with respect to growth rate (Figure 4.7c), phase (Figure 4.7d) and film composition. It can be seen that a steep increase in film growth rate occurred when the  $\text{NH}_3$  partial pressure was increased from 0 to 0.44 Torr. Without the addition of ammonia,  $\text{Cu}_2\text{O}$  was deposited. The growth rate of  $\text{Cu}_2\text{O}$  was found to be 2-3 times lower than for  $\text{Cu}_3\text{N}$  deposition, which might be due to differences in etching behaviour towards the  $\text{Hhfac}$  reaction products or differences in adsorption behaviour for  $\text{Cu}_3\text{N}$  and  $\text{Cu}_2\text{O}$  towards the precursors. At higher  $\text{NH}_3$  partial pressures only the  $\text{Cu}_3\text{N}$  phase was observed.

However, according to the XPS investigation, film composition varied for the films deposited with different ammonia partial pressures. Moreover, differences in film composition between the water-based [ $\text{Cu}(\text{hfac})_2/\text{H}_2\text{O}/\text{NH}_3$ ] and water-free [ $\text{Cu}(\text{hfac})_2/\text{NH}_3$ ] process were detected. (The films in the water-free process were prepared by adding water during the first 75 out of a total of 750 cycles to initiate the film growth.) After argon sputtering, it was found that films deposited with water included in the process were almost free of carbon impurities. This was true for all applied ammonia partial pressures. The amount of carbon was small and hardly distinguishable from the background. Thus, it is probable that the total amount of carbon was less than 1 at% in the films deposited with the water-based process. On the contrary, much larger carbon content was detected in the film deposited without including water in the growth process. The carbon content was approximately four times as high as in the water free process. (An absolute value of the carbon content was measured to 2 at%.) Hence, the differences in carbon content between the two deposition processes indicated that the addition of water led to surface reactions where the hfac ligands were kept intact during the adsorption and/or surface reactions in the ALD scheme. However, it was found that the  $\text{Cu}_3\text{N}$  films contained oxygen in the bulk. The copper to oxygen ratio in the films was determined by using CVD produced  $\text{Cu}_2\text{O}$  films as standards [IV]. The oxygen content in the water-based films was calculated to range from 3.7 to 5.2 at%, whereas films deposited without the addition of water contained 2.3 at% oxygen content. One possible explanation for the oxygen content in the water free films might be due to that the  $\text{Cu}(\text{hfac})_2$  ligands were not stable during the water free deposition process. Thus, the oxygen content may originate from the

precursor ligands themselves. Finally, the oxygen content could not be lowered by adding hydrogen gas as an extra hydrogen source during the ammonia pulse. This result is consistent with the fact that phase pure copper films could not be produced by applying a  $\text{Cu}(\text{hfac})_2/\text{H}_2\text{O}/\text{H}_2$  pulse sequence at temperatures below 300 °C.

Valuable information regarding possible deposition pathways in the  $\text{Cu}_3\text{N}$  growth process was obtained by a QCM study. A brief overview of the QCM parameters and mass calculations was given in section 2.1.3. In previous sections, indications that reaction products such as HCl or Hhfac may evolve during several steps in the ALD cycle have been mentioned. Thus, the mass changes (measured by QCM) may differ if the  $\text{Cu}(\text{hfac})_2$  precursor reacts from the gas phase with different surface species of  $-\text{NH}_x$  and/or  $-\text{OH}$ , or if the hfac ligands leave the surface when water and/or ammonia react with adsorbed  $\text{Cu}(\text{hfac})_2$ . (Large mass differences between different deposition pathways are expected due to the fact that the hfac ligand is heavy, 200 u, as compared to 63.5 u for copper.) For  $\text{Cu}_3\text{N}$  growth on  $\text{Cu}_3\text{N}$ , three simple theoretical film growth models can be constructed and later on, compared to measured experimental data. The first film growth model (R1) is based on dissociative adsorption of  $\text{Cu}(\text{hfac})_2$ , which has been proposed as mechanism for growth of copper metal [80]. Secondly, an adsorption reaction (R2) is considered where one of the precursor ligands reacts with a surface group prior to adsorption. Finally, a  $\text{Cu}(\text{hfac})_2$  adsorption reaction where both ligands are removed prior to adsorption is treated (R3). The three adsorption reactions can be written as:



For all proposed mechanisms,  $\text{Cu}_3\text{N}$  is assumed to be the final film product, where one  $\text{Cu}(\text{hfac})_2$  molecule can produce  $1/3\text{Cu}_3\text{N}$  formula unit. Thus, by calculating a mass ratio between the amount of adsorbed material after the  $\text{Cu}(\text{hfac})_2$  pulse ( $M_1$ ) and  $1/3\text{Cu}_3\text{N}$  ( $M_0$ ), indications of a possible growth mechanism may be found when the quotients are compared to measured QCM data. The theoretical mass ratios are calculated according to:

$$\text{R1: } \frac{M_0}{M_1} = \frac{\frac{1}{3}\text{Cu}_3\text{N}(s)}{\text{Cu}(\text{hfac})(ad) + \text{hfac}(ad)} \approx 0,15 \quad (4.4)$$

$$\text{R2: } \frac{M_0}{M_1} = \frac{\frac{1}{3}\text{Cu}_3\text{N}(s)}{\text{Cu}(\text{hfac})(\text{ad}) - H} \approx 0,26 \quad (4.5)$$

$$\text{R3: } \frac{M_0}{M_1} = \frac{\frac{1}{3}\text{Cu}_3\text{N}(s)}{\text{Cu}(\text{ad}) - 2H} \approx 1,1 \quad (4.6)$$

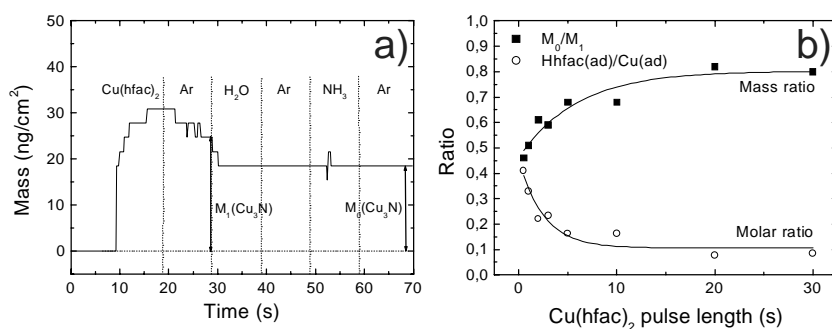


**Figure 4.8.** QCM data for the  $\text{Cu}(\text{hfac})_2/\text{H}_2\text{O}/\text{NH}_3$  process. a) Mass change during one 10:10:10:10:10 s ALD cycle and b) mass and molar ratios for different  $\text{Cu}(\text{hfac})_2$  pulse times (x) by using an x:10:10:10:10:10 pulse sequence. The lines are guides for the eye.

$\text{Cu}_3\text{N}$  growth data obtained by QCM are shown in Figure 4.8 for films grown at 253 °C. It can be seen that a rapid mass increase occurred at the beginning of the  $\text{Cu}(\text{hfac})_2$  pulse (Figure 4.8a). After the initial mass increase the mass continued to increase until the  $\text{Cu}(\text{hfac})_2$  pulse was stopped. During the following argon purge a mass decrease was observed due to desorption. Furthermore, an additional mass decrease occurred when the water pulse was applied, probably generated by removal of adsorbed hfac ligands by desorption of  $\text{Hhfac}(\text{g})$ . Thereafter, no major mass differences were observed, neither during any of the remaining argon pulses or during the ammonia pulse. This indicated that almost all of the remaining heavier hfac ligands, were removed during the water pulse. It should also be noted that the mass difference between surface  $-\text{NH}_x$  and  $-\text{OH}$  groups could not be measured due to the small mass difference. It can be seen that the  $M_0/M_1$  ratio ranged from 0.45 to 0.85 when the  $\text{Cu}(\text{hfac})_2$  pulse length increased from 0.5 to 30 s (Figure 4.8b). The mass quotients indicated that film growth, following a reaction such as R1, was unlikely, even if the  $M_1$  mass is defined as the maximum value obtained during the  $\text{Cu}(\text{hfac})_2$  pulse.

(Thus, disregarding desorption of adsorbed species from the surface.) Furthermore, the amount of adsorbed hfac ligands in comparison with the total amount of adsorbed copper during each cycle was calculated according to:

$$\frac{n(\text{hfac}_{ad})}{n(\text{Cu}_{ad})} = \frac{\frac{\Delta M}{M(\text{Hhfac})}}{\frac{M_0}{M(\frac{1}{3}\text{Cu}_3\text{N})}} \quad (4.7)$$

where  $\Delta M$  is defined as the mass loss during the water pulse. All mass loss is assumed to originate from hfac ligands leaving as Hhfac. The corresponding data are shown in Figure 4.8b, where it can be seen that the  $n(\text{hfac}_{ad})/n(\text{Cu}_{ad})$  ratio range from 0.4 to 0.1 when the  $\text{Cu}(\text{hfac})_2$  pulse length increases from 0.5 to 30 s. Corresponding values for R1, R2 and R3 are 2, 1 and 0, respectively. Hence, at shorter  $\text{Cu}(\text{hfac})_2$  pulse lengths an average between R2 and R3, in terms of amount of adsorbed hfac was observed. At longer pulse lengths, the process was shifted against less hfac per copper ad-atoms, i.e. closer to R3. It should also be added that the mass increase during the  $\text{Cu}(\text{hfac})_2$  pulse never terminated for pulses up to 30 s long, whereas the amount released Hhfac during the water pulse became constant. Therefore, the calculated data may be influenced by thermal decomposition of the  $\text{Cu}(\text{hfac})_2$  precursor. In a thermal decomposition process, the mass increase is linear versus the exposure time. However, the mass increase per second never reached a constant value during the  $\text{Cu}(\text{hfac})_2$  pulse. Thus, the contribution from thermal decomposition could be estimated to be less than  $0.4 \text{ ngs}^{-1}\text{cm}^{-2}$  ( $0.006 \text{ \AA/s}$ ) by comparing the mass increase between the two longest  $\text{Cu}(\text{hfac})_2$  pulse lengths, 20 and 30 s.

## 5 Summary and concluding remarks

It is well known that deposition of non-oxide films on oxide substrates can be difficult by chemical methods such as ALD. In this work, an alternative deposition pathway, using the concept of intermediate water pulses, have been introduced and evaluated for ALD film growth of copper metal and copper(I) nitride. Oxides such as fused silica and single crystalline aluminium oxide were used as substrates. The films were grown by using two different copper source materials, copper(I) chloride and copper(II) hexafluoroacetylacetonate. The CuCl process can be viewed as a high temperature process, whereas the Cu(hfac)<sub>2</sub> is a low temperature process. For both precursors, the initial reaction was deposition of Cu<sub>2</sub>O by adding water to the ALD pulse sequence. After the water pulse, an extra precursor was added to the ALD pulse sequence, hydrogen gas or ammonia, for deposition of Cu and Cu<sub>3</sub>N, respectively. Film deposition with the water-based pulse sequence was compared to Cu and Cu<sub>3</sub>N film growth by direct reaction between the copper precursors and H<sub>2</sub>/NH<sub>3</sub>. For both copper source materials, differences were observed between the water-based and water-free deposition processes.

For successful deposition of Cu<sub>3</sub>N, it was found that the intermediate water pulses were necessary to initiate the film growth on the oxide substrates. Differences in film composition occurred between the two deposition pathways, where the films in the water-based process contained more oxygen and less carbon than for films grown with the water-free process. The Cu<sub>3</sub>N growth rate on Cu<sub>3</sub>N was similar for the water-based and water-free deposition schemes. Moreover, the film growth rates in the water-based process were the same on both substrate types. QCM data regarding the growth mechanism suggested the Cu(hfac)<sub>2</sub> precursor lost more than 1.5 of its ligands on average upon adsorption or surface reactions during the Cu(hfac)<sub>2</sub> pulse. Hence, only a minor part of the hfac ligands remained on the surface at the beginning of the water or ammonia pulses. Furthermore, the metastability of the Cu<sub>3</sub>N compound was used for a possible metallisation application. By short annealing the Cu<sub>3</sub>N films at temperatures above 300 °C, films of metallic copper were obtained. The Cu films on SiO<sub>2</sub> substrates showed resistivity values down to 4 μΩcm for a 50 nm thick film. In comparison, no resistivity values could be obtained for directly grown copper films due to the fact that the films were not intact on the oxide substrates. Finally, when epitaxial {111} oriented Cu<sub>3</sub>N films were annealed,

{111} oriented Cu films with the same in-planar orientational relationship was obtained.

In the CuCl processes, films of Cu<sub>2</sub>O and Cu were prepared. The copper films were deposited by using hydrogen gas as reducing agent. For the water-based process, the copper growth rates were found to be higher on the  $\alpha$ -Al<sub>2</sub>O<sub>3</sub> substrates than on the SiO<sub>2</sub> substrates. Furthermore, the copper growth rates on the alumina substrates increased by the water addition at all deposition temperatures, except for the highest one, 475 °C. The opposite trend was found on the SiO<sub>2</sub> substrates where the water-free deposition process yielded higher growth rates at all deposition temperatures except for the lowest one, 375 °C. Moreover, the copper films were not intact due to high diffusion of copper at the deposition temperatures in the CuCl processes. It was found that the film growth conditions for the Cu<sub>2</sub>O process was far from ideal due to severe etching by the HCl reaction product. As a result, a large thickness profile existed in the deposition zone, where the films in the downstream of the reactor were markedly thinner. Due to the higher deposition temperatures in the CuCl process, in-situ characterisation with methods such as QCM was problematic. Instead, DFT calculations were used to give an indication of a possible growth mechanism for the Cu<sub>2</sub>O process. It was found that reactions during the CuCl pulse (by CuCl reacting from the gas phase with adsorbed hydroxyl groups) were the most favourable deposition pathway for growth of Cu<sub>2</sub>O on Cu<sub>2</sub>O. For both Cu and Cu<sub>2</sub>O, randomly oriented films were obtained on the SiO<sub>2</sub> substrates. Epitaxial films were obtained on the  $\alpha$ -Al<sub>2</sub>O<sub>3</sub> substrates, {111} and {110} oriented for Cu and Cu<sub>2</sub>O, respectively.

In the future, it would be interesting to examine if the concept of intermediate water pulses can be used for growing other metal nitrides. The largest chance for success ought to be found in systems where the difference between the oxide and nitride stability is as small as possible. That is, by converting a surface oxide layer to a nitride layer during each subsequent ALD cycle, the difference in stability between the oxide and the nitride should not be too large as compared to the difference between water and ammonia. Another effect of the added water may have is that it provides a smooth way of removing metal-organic ligands intact. Therefore, the possibility of using a more reactive second precursor may exist due to that the adsorbed fragile organic ligands have already been removed by the water. As an example, pulsed plasma processes can be mentioned, where a hydrogen plasma is used in conjunction with carbon containing precursors. However, film contamination is usually a problem when the radicals react directly with the metal containing precursor. Moreover it would be interesting to investigate if the reaction pathways can be used to grow other phases such as carbides, for example, by first depositing a nitride and so on.

Applications for the Cu<sub>3</sub>N phase as well as other far right d-block metal nitrides have only been briefly studied. Indications exist that the band gap of

$\text{Cu}_3\text{N}$  can be varied by altering the amount of oxygen in the films. Furthermore, film growth of a metastable nitrides, followed by a short anneal to produce a metal films might be useful, especially when compared to direct deposition of metal films on unfavourable substrates such as oxides. Finally, it would be of interest to test if the  $\text{Cu}_3\text{N}$  process has any potential use for copper metallisation. Since different nitride barrier materials are commonly used for growing copper metal, it should be interesting to study and compare the nitride on nitride barrier growth as compared to the direct metal growth, which is usually done via a metallic nucleation layer. This study should also be coupled to a more in depth investigation of the annealing process.

## 6 Acknowledgements

First of all, I would like to express my gratitude to my supervisor Prof. Jan-Otto Carlsson for giving me the opportunity to complete this education. During the years, there have been many stimulating and greatly valuable discussions from which I have learnt a lot.

I am most grateful to my co-supervisors, Prof. Karin Larsson for being supportive and knowledgeable throughout my time as a theoretical chemist and Dr. Mikael Ottosson for his highly skilful and huge support during my experimental work.

All co-authors in different collaborations and the competent XPS personnel that have helped me during the years are greatly acknowledged. In alphabetical order:

Prof. Mats Boman  
Dr. Hans Högberg  
Ph. D. candidate Anders Johansson  
Dr. Jun Lu.  
Dr. Lars Norin  
Ph. D. candidate Ola Wilhelmsson

The skilful work of the administrative and technical staff is also greatly acknowledged, special thanks to Jan Bohlin for masterfully manufacturing many parts of my ALD reactors.

I wish to address my colleagues and friends, past and present at the Department of Materials Chemistry, the Mat-Nat crew and the E-tuna gang.

Jag vill även säga att min familj (Eva, Åke, mor- och farföräldrar, m.fl.) har varit viktig för mig under alla dessa år.

Financial support from the Swedish Research Council and C F Liljewalchs resestipendier is gratefully acknowledged.

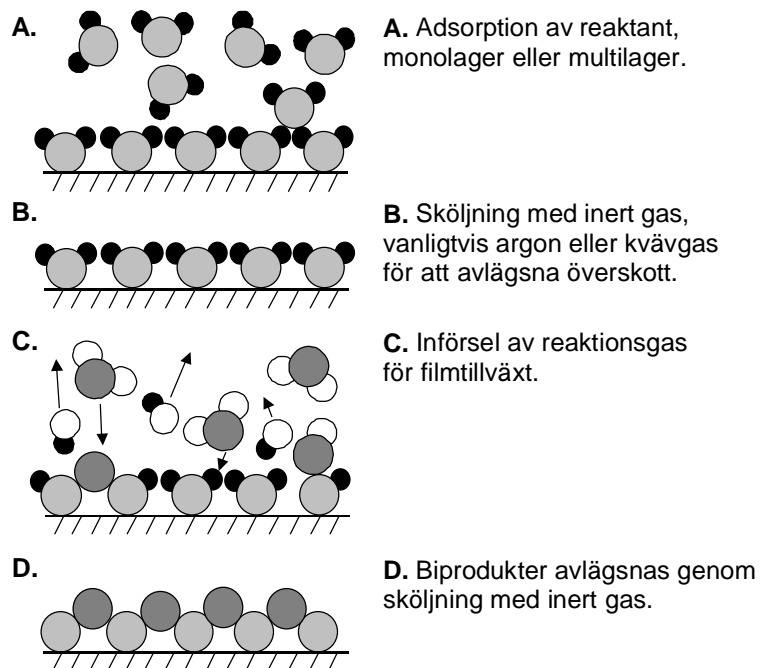
/ T.T.

Uppsala, October 2004

## 7 Svensk sammanfattning

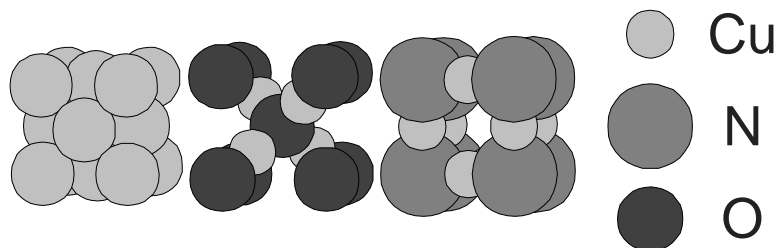
Genom att belägga en yta med tunna lager eller så kallade filmer av olika material kan egenskaperna för den belagda ytan ändras fundamentalt, jämfört med den icke belagda ytan. I alla beläggningsprocesser är god kunskap om hur processen fungerar, dvs. hur själva filmtillväxten sker viktig, därför att utan denna kunskap kan de önskade filmegenskaperna ej kontrolleras på önskat sätt. För att skapa dessa intressanta ytlager används många olika kemiska och fysikaliska beläggningsmetoder, alla med sina specifika för- och nackdelar. Den beläggningsmetod som använts för att producera filmerna i det här arbetet heter Atomic Layer Deposition (ALD). ALD är en deponeringsmetod där filmerna tillväxer via kemiska reaktioner på eller i närheten av den yta som ska beläggas under tryck som ofta är mellan 100 till 1000 gånger lägre än atmosfärstryck. Vidare deponeras filmerna genom att reaktanterna tillförs via gasfasen till en beläggningszon. För att erhålla filmtillväxt måste även aktivering ske. Detta sker oftast genom att värma zonen där filmtillväxten äger rum. ALD-metoden passar bäst för framställning av mycket tunna skikt (ända ner till några få lager av atomer). Det innebär också att tjockleken på skikten kan kontrolleras synnerligen noggrant. Utmärkande för metoden är också att alla ytor som exponeras för reaktionsgasen beläggs och att skiktens sammansättning blir praktiskt taget densamma över hela ytan.

ALD är en sekventiell metod, vilket innebär att reaktanterna tillförs deponeringszonen en i taget för att undvika reaktioner mellan reaktanterna i gasfasen innan provytan där filmen ska växa. Varje gång reaktanterna pulsas in i reaktorn erhålls en viss filmtillväxt. Skiktjockleken bestäms av antalet pulser. En schematisk bild på ett pulsschema som innehåller fyra pulser i en godtycklig ALD-process visas i Figur 7.1. Sekvensen innehåller en puls för respektive utgångsmaterial (2 st) och två sköljpulser.



**Figur 7.1** Schematisk bild av en ALD-cykel för filmtillväxt av en godtycklig film. Reaktanterna tillförs i A och C. Sköljning med inert gas inträffar i B och D. Efter en pulssekvens A-D har ett lager film erhållits på ytan.

I det här arbetet har tunna filmer av koppar (Cu), kopparoxid ( $\text{Cu}_2\text{O}$ ) och kopparnitrid ( $\text{Cu}_3\text{N}$ ) deponerats. Filmerna har belagts på två olika oxidsubstrat, utgående ifrån två olika kopparinnehållande material, kopparklorid ( $\text{CuCl}$ ) och kopparhexafluoroacetylacetonat [ $\text{Cu}(\text{hfac})_2$ ]. All filmtillväxt baserad på kopparkloriden har utförts mellan 350 och 700 °C, medan temperaturen i  $\text{Cu}(\text{hfac})_2$ -processerna har varierats mellan 210 och 302 °C. Skillnaden i uppbyggnad på atomär nivå mellan de tre olika materialen (faserna) visas i Figur 7.2.



**Figur 7.2** Kristallstrukturer av de i avhandlingen deponerade faserna. Koppar (Cu) till vänster, kopparoxid ( $\text{Cu}_2\text{O}$ ) i mitten samt kopparnitrid ( $\text{Cu}_3\text{N}$ ) till höger.

Det har tidigare visat sig vara svårt att belägga oxidtyper med andra material än oxider, icke-oxider, med ALD metoden. Med icke-oxider menas

material som inte innehåller något syre. Huvudinnehållet i den här avhandlingen har varit att utveckla och undersöka alternativa deponeringsvägar för filmtillväxt av icke-oxider på oxidmaterial. Genom att addera vattenpulser i processen visas att existerande deponeringsvägar ändras avsevärt. Den grundläggande tanken bakom de extra vattenpulserna är att filmtillväxten först sker via bildandet av ett oxidlager när det metallinnehållande utgångsmaterialet reagerar med vatten. Efter vattenpulsen tillförs en tredje reaktant för att förbruka det nyligen bildade oxidlagret och bilda den önskade fasen. I teorin bildas ett nytt oxidlager varje gång ALD-pulssekvensen upprepas. De framställda filmerna har karakteriserats med en mängd analysmetoder och tillväxtmekanismerna har studerats både experimentellt under tiden då filmerna tillväxer samt genom modellering med kvantmekaniska metoder.

För deponering av  $\text{Cu}_3\text{N}$  från  $\text{Cu}(\text{hfac})_2$  och ammoniak ( $\text{NH}_3$ ) var den extra vattenpulsen nödvändig för att initiera filmtillväxten på de två substratytorna, kiseloxid och aluminiumoxid. När väl en heltäckande film av  $\text{Cu}_3\text{N}$  erhållits märktes ingen skillnad på tillväxthastigheten med eller utan vatten. Däremot lämnade filmdeponeringen utan vatten mer kolföroreningar kvar i filmerna medan mer syre fanns kvar i filmerna med den vattenbaserade processen.  $\text{Cu}_3\text{N}$ -fasen är även metastabil, vilket innebär att den kunde fasomvandlas till metallisk koppar genom uppvärmning i temperaturer över  $300\text{ }^\circ\text{C}$ . De värmebehandlade kopparnitridfilmerna visade mycket bättre ledningsförmåga än direktdeponerade kopparfilmer på oxidsubstraten. Kopparfilmer deponerades även från  $\text{CuCl}$  och  $\text{H}_2$ , med resp. utan vattenpulser. Stora skillnader observerades för filmtillväxt med och utan vatten men också mellan filmtillväxt på de två olika substraten,  $\text{SiO}_2$  och  $\alpha\text{-Al}_2\text{O}_3$ .

Potentiella användningsområden för de ytbeläggningar som framställts i detta arbete är tunna ledande lager (Cu), katalys ( $\text{Cu}_2\text{O}$ ) och halvledare ( $\text{Cu}_3\text{N-Cu}_2\text{O}$ ). Ett exempel är processorer i datorer, där koppar används på grund av sin låga resistivitet, dvs. sin förmåga att leda ström med så små förluster som möjligt. För att kunna tillverka mindre och mindre komponenter ökar också kraven på deponeringsmetoderna och processerna med vilka de producerade tunna skikten tillverkas. Bland tänkbara användningsområden för  $\text{Cu}_3\text{N}$  kan solenergitillämpningar och optiska minnen nämnas. Slutligen ska sägas att i takt med att behovet av extremt tunna filmer ökar kommer de framställningsprocesser, som utnyttjar kemin i gränssytor, allt mer i förgrunden. ALD är just en sådan process för framtiden.

## 8 References

- [1] J. L. Vossen, W. Kern, eds., *Thin Film Processes II*, Academic Press, San Diego, Ca, 1991.
- [2] J.-O. Carlsson, *Films and Coatings for Technology*, ed: R. Bunshah, Noyes Publications, Park Ridge, NJ, 1994, p.374.
- [3] T. Suntola, J. Antson, US patent no.4,058,430 (1977).
- [4] M. Ritala, M. Leskelä, *Handbook of Thin Film Materials*, ed: H. S. Nalwa, Academic Press, San Diego, 2001, Vol. 1, Chapter 2.
- [5] T. Suntola, M. Simpson, eds., *Atomic Layer Epitaxy*, Blackie and Son Ltd, Glasgow, 1990.
- [6] G. Aylward, T. Findlay, *SI Chemical Data 3rd Ed.*, John Wiley and Sons, Singapore, 1994.
- [7] C.-M. Chiang, T. M. Miller, L. H. Dubois, *J. Phys. Chem.* 97 (1993) 11781.
- [8] B. Zheng, C. Goldberg, E. T. Eisenbraun, J. Liu, A. E. Kaloyeros, P. J. Toscano, S. P. Murarka, J. F. Loan, J. Sullivan, *Mater. Chem. Phys.* 41 (1995) 173.
- [9] M. B. Naik, W. N. Gill, R. H. Wentorf, R. R. Reeves, *Thin Solid Films* 262 (1995) 60.
- [10] N. S. Borgharkar, G. L. Griffin, H. Fan, A. W. Maverick, *J. Electrochem. Soc.* 146 (1999) 1041.
- [11] G. Z. Sauerbrey, *Phys.* 155 (1959) 206.
- [12] M. Juppo, A. Rahtu, M. Ritala, M. Leskelä, *Langmuir* 16 (2000) 4034.
- [13] R. G. Parr, W. Yang, *Density-Functional Theory of Atoms and Molecules*, Oxford Science Publications, NY, 1989.

- [14] M. C. Payne, M. P. Teter, D. C. Allan, T. A. Arias, J. D. Joannopoulos, *Rev. Mod. Phys.* 64 (1992) 1045.
- [15] M. D. Segall, P. J. D. Lindan, M. J. Probert, C. J. Pickard, P. J. Hasnip, S. J. Clark, M. C. Payne, *J. Phys.: Condens. Matter* 14 (2002) 2717.
- [16] J. P. Perdew, Y. Wang, *Phys. Rev. B* 45 (1992) 13244.
- [17] H. J. Monkhorst, J. D. Pack, *Phys. Rev. B* 13 (1976) 5188.
- [18] J.-Y. Kim, Y.-K. Lee, H.-S. Park, J.-W. Park, D.-K. Park, J.-H. Joo, W.-H. Lee, Y.-K. Ko, P. J. Reucroft, B.-R. Cho, *Thin Solid Films* 330 (1998) 190.
- [19] A. V. Gelatos, R. Marsh, M. Kottke, C. J. Mogab, *Appl. Phys. Lett.* 63 (1993) 2842.
- [20] H. A. Marzouk, J. Y. Kim, J. S. Kim, P. J. Reucroft, R. J. Jacob, J. D. Robertson, C. Eloi, *Thin Solid Films* 249 (1994) 27.
- [21] C. A. N. Fernando, S. K. Wetthasinghe, *Sol. Energ. Mater. Sol. Cells* 63 (2000) 209.
- [22] T. Maruyama, *Jpn. J. Appl. Phys.* 37 (1998) 4099.
- [23] S. Ishizuka, T. Maruyama, K. Akimoto, *Jpn. J. Appl. Phys. Part 2 Letter* 39 (2000) L786.
- [24] V. Georgieva, M. Ristov, *Sol. Energ. Mater. Sol. Cells* 73 (2002) 67.
- [25] J. P. Espinos, J. Morales, A. Barranco, A. Caballero, J. P. Holgado, A. R. Gonzalez-Elipe, *J. Phys. Chem. B* 106 (2002) 6921.
- [26] J. Ramirez-Ortiz, T. Ogura, J. Medina-Valtierra, S. E. Acosta-Ortiz, P. Bosch, J. Antonio de los Reyes, V. H. Lara, *Appl. Surf. Sci.* 174 (2001) 177.
- [27] J. A. Sullivan, *Catal. Lett.* 79 (2002) 59.
- [28] N. Tabuchi, H. Matsumura, *Jpn. J. Appl. Phys.* 1 41 (2002) 5060.
- [29] K. Ogawa, T. Itoh, K. Maki, *Phys. Rev. B* 62 (2000) 4269.
- [30] S. Ghosh, D. K. Avasthi, P. Shah, V. Ganesan, A. Gupta, D. Sarangi, R. Bhattacharya, W. Assmann, *Vacuum* 57 (2000) 377.

- [31] G. G. Codorelli, G. Malandrino, I. L. Fragala, *Chem. Vap. Deposition* 5 (1999) 21.
- [32] M. Ottosson, J.-O. Carlsson, *Surf. Coat. Technol.* 78 (1996) 263.
- [33] H. Holzschuh, H. Suhr, *Appl. Phys. A* 51 (1990) 486.
- [34] P. R. Markworth, X. Liu, J. Y. Dai, W. Fan, T. J. Marks, R. P. H. Chang, *J. Mater. Res.* 16 (2001) 2408.
- [35] G. Krabbes, H. Oppermann, *Krist. Tech.* 12 (1977) 1099.
- [36] K. Uwai, *J. Cryst. Growth* 112 (1991) 298.
- [37] S. Kim, D.-J. Choi, K.-R. Yoon, K.-H. Kim, S.-K. Koh, *Thin Solid Films* 311 (1997) 218.
- [38] N. Awaya, K. Ohno, Y. Arita, *J. Electrochem. Soc.* 142 (1995) 3173.
- [39] J. R. Creighton, J. E. Parmeter, *Crit. Rev. Solid Mater. Sci.* 18 (1993) 175.
- [40] A. E. Kaloyeros, M. A. Fury, *MRS Bull.* 18 (1993) 6.
- [41] H. J. Jin, M. Shiratani, T. Kawasaki, T. Fukuzawa, T. Kinoshita, Y. Watanabe, H. Kawasaki, M. Toyofuku, *J. Vac. Sci. Technol. A* 17 (1999) 726.
- [42] J. Huo, R. Solanki, A. McAndrew, *J. Mater. Res.* 17 (2002) 2394.
- [43] P. Mårtensson, J.-O. Carlsson, *Chem. Vap. Deposition* 3 (1997) 45.
- [44] M. Utriainen, M. Kröger-Laukkanen, L.-S. Johansson, L. Niinistö, *Appl. Surf. Sci.* 157 (2000) 151.
- [45] M. Juppo, M. Ritala, M. Leskelä, *J. Vac. Sci. Technol. A* 15 (1997) 2330.
- [46] P. Mårtensson, J.-O. Carlsson, *J. Electrochem. Soc.* 145 (1998) 2926.
- [47] B. S. Lim, A. Rahtu, R. G. Gordon, *Nature Mater.* 2 (2003) 749.
- [48] S. K. Lakshmanan, W. N. Gill, *J. Vac. Sci. Technol. A* 16 (1998) 2187.
- [49] G. Katz, *Appl. Phys. Letters* 12 (1968) 161.
- [50] P. J. Moller, Q. Guo, *Thin Solid Films* 201 (1991) 267.
- [51] H. Bialas, K. Heneka, *Vacuum* 45 (1994) 79.
- [52] H. Bialas, E. Knoll, *Vacuum* 45 (1994) 959.

- [53] G. Dehm, M. Ruhle, G. Ding, R. Raj, *Philos. Mag. B* 71 (1995) 1111.
- [54] C. A. M. Mulder, J. T. Klomp, *J. Phys. Colloq.* 46 (1985) 111.
- [55] E. Knoll, H. Bialas, *Thin Solid Films* 250 (1994) 42.
- [56] J. E. Ayers, *J. Cryst. Growth* 135 (1994) 71.
- [57] R. E. Reed-Hill, R. Abbaschian, *Physical Metallurgy Principles*, PWS Publishing Company, Boston, 1994, p. 550.
- [58] T. Maruyama and T. Morishita, *J. Appl. Phys.* 78 (1995) 4104.
- [59] L. Soukup, M. Sicha, F. Fendrych, L. Jastrabik, Z. Hubicka, D. Chvostova, H. Sichova, V. Valvoda, A. Tarasenko, V. Studnicka, T. Wagner, M. Novak, *Surf. Coat. Technol.* 116-119 (1999) 321.
- [60] T. Nosaka, M. Yoshitake, A. Okamoto, S. Ogawa, Y. Nakayama, *Thin Solid Films* 348 (1999) 8.
- [61] K. J. Kim, J. H. Kim, J. H. Kang, *J. Cryst. Growth* 222 (2001) 767.
- [62] S. Ghosh, F. Singh, D. Choudhary, D. K. Avasthi, V. Ganesan, P. Shah, A. Gupta, *Surf. Coat. Technol.* 142-144 (2001) 1034.
- [63] D. M. Borsa, D. O. Boerma, *Surf. Sci.* 548 (2004) 95.
- [64] *Handbook of Chemistry and Physics* 52 Ed, ed: R. C. Weast, The Chemical Rubber Company, Cleveland, Ohio, 1971.
- [65] M. Asano, K. Umeda, A. Tasaki, *Jpn. J. Appl. Phys.* 29 (1990) 1985.
- [66] T. Nosaka, M. Yoshitake, A. Okamoto, S. Ogawa, Y. Nakayama, *Appl. Surf. Sci.* 169-170 (2001) 358.
- [67] L. Maya, *Mater. Res. Soc. Symp. Proc.* 282 (1993) 203.
- [68] R. Cremer, M. Witthaut, D. Neuschultz, C. Trappe, M. Laurenzis, O. Winkler, H. Kurz, *Mikro. Acta* 133 (2000) 299.
- [69] S. Terada, H. Tanaka, K. Kubota, *J. Cryst. Growth* 94 (1989) 567.
- [70] L. Maya, *J. Vac. Sci. Technol. A* 11 (1993) 604.
- [71] Z. Q. Liu, W. J. Wang, T. M. Wang, S. Chao, S. K. Zheng, *Thin Solid Films* 325 (1998) 55.
- [72] S. O. Chwa, K. H. Kim, *J. Mater. Sci. Lett.* 17 (1998) 1835.
- [73] G. Soto, J. A. Diaz, W. de la Cruz, *Materials Letters* 57 (2003) 4130.

- [74] M. Ritala, M. Leskelä, E. Nykänen, P. Soininen, L. Niinistö, *Thin Solid Films* 225 (1993) 288.
- [75] R. Matero, A. Rahtu, M. Ritala, M. Leskelä, T. Sajavaara, *Thin Solid Films* 368 (2000) 1.
- [76] S. M. George, A. W. Ott, J. W. Klaus, *J. Phys. Chem.* 100 (1996) 13121.
- [77] J. Aarik, K. Kukli, A. Aidla, L. Pung, *Appl. Surf. Sci.* 103 (1996) 331.
- [78] V. M. Gun'ko, V. I. Zarko, B. A. Chuikov, V. V. Dudnik, Y. G. Ptushinski, E. F. Voronin, E. M. Pakhlov, A. A. Chuiko, *Int. J. Mass Spectrom. Ion process.* 172 (1998) 161.
- [79] D. F. Cox, K. H. Shulz, *Surf. Sci.* 256 (1991) 67.
- [80] S. L. Cohen, M. Liehr, S. Kasi, *Appl. Phys. Lett.* 60 (1992) 50.





# Acta Universitatis Upsaliensis

*Comprehensive Summaries of Uppsala Dissertations  
from the Faculty of Science and Technology*

Editor: The Dean of the Faculty of Science and Technology

---

A doctoral dissertation from the Faculty of Science and Technology, Uppsala University, is usually a summary of a number of papers. A few copies of the complete dissertation are kept at major Swedish research libraries, while the summary alone is distributed internationally through the series *Comprehensive Summaries of Uppsala Dissertations from the Faculty of Science and Technology*. (Prior to October, 1993, the series was published under the title “Comprehensive Summaries of Uppsala Dissertations from the Faculty of Science”.)

## Distribution:

Uppsala University Library  
Box 510, SE-751 20 Uppsala, Sweden  
[www.uu.se](http://www.uu.se), [acta@ub.uu.se](mailto:acta@ub.uu.se)

ISSN 1104-232X  
ISBN 91-554-6081-X